Geochemistry of volcanic and plutonic rocks from the Nahlin ophiolite with implications for a Permo-Triassic arc in the Cache Creek terrane, northwestern British Columbia

Siobhan McGoldrick, Alex Zagorevski, Dante Canil

2017

Canadian Journal of Earth Sciences
Revue canadienne des sciences de la Terre

Geochemistry of volcanic and plutonic rocks from the Nahlin ophiolite with implications for a Permo-Triassic arc in the Cache Creek terrane, northwestern British Columbia

Journal:	*Canadian Journal of Earth Sciences*
Manuscript ID	cjes-2017-0069.R1
Manuscript Type:	Article
Date Submitted by the Author:	05-Jul-2017
Complete List of Authors:	McGoldrick, Siobhan; School of Earth and Ocean Sciences Zagorevski, Alex; Geological Survey of Canada Canil, Dante; School of Earth and Ocean Sciences
Is the invited manuscript for consideration in a Special Issue? :	N/A
Keyword:	igneous rocks, ophiolite, arc, geochemistry, Cordillera

Geochemistry of volcanic and plutonic rocks from the Nahlin ophiolite with implications for a Permo-Triassic arc in the Cache Creek terrane, northwestern British Columbia

S. McGoldrick, School of Earth and Ocean Sciences, University of Victoria, Victoria, BC, **smcgold@uvic.ca**

A. Zagorevski, Geological Survey of Canada, Ottawa, ON **alex.zagorevski@canada.ca**

D. Canil*, School of Earth and Ocean Sciences, University of Victoria, Victoria, BC **dcanil@uvic.ca**

- corresponding author
-

Keywords: *Cache Creek, terrane, geochemistry, volcanic rocks, ophiolite, arc, subduction zone, Cordillera*

Abstract

In northwestern British Columbia, the Permian Nahlin ophiolite in the northern Cache Creek terrane comprises spinel harzburgite tectonite with minor lherzolite, lower crustal mafic and ultramafic cumulates, gabbroic rocks including dikes intruding mantle harzburgite, and basaltic volcanic and volcaniclastic rocks. New lithogeochemical data from the Menatatuline Range area confirm that plutonic and volcanic rocks of the ophiolite are tholeiitic and arc-related, while only a minor component of volcanic rocks are alkaline intraplate basalts. Tholeiitic basalts of the Nahlin ophiolite represent the products of 2 - 20% fractional melting, and their complementary residue may be peridotite from the ophiolite mantle section. Correlative tholeiitic volcanic sections can be found elsewhere in the northern Cache Creek terrane, and may be linked to a regionally extensive (~200 km) intraoceanic arc. The arc tholeiite geochemistry of the plutonic and volcanic rocks, and the highly depleted nature of the mantle residues imply that the Nahlin ophiolite formed in a supra-subduction zone (SSZ) environment. The Nahlin ophiolite therefore occupied the upper plate during intraoceanic collision prior to emplacement of the Cache Creek terrane. The volumetrically minor OIB-type volcanic rocks in the northern Cache Creek terrane are associated with carbonate successions bearing Tethyan fauna. These sequences are likely fragments of oceanic plateaux and their carbonate atolls sliced off of the subducting plate, and are unrelated to the Nahlin ophiolite - arc system.

Introduction

Ophiolites are ubiquitous features of Phanerozoic orogens where they represent fragments of oceanic lithosphere preserved along suture zones. Upper Paleozoic–Lower Mesozoic ophiolites exposed throughout the Canadian Cordillera are commonly interpreted to mark remnants of closed ocean basins (e.g., Tempelman-Kluit 1979, Ash and Arksey 1990,

Struik et al. 2001). The Cache Creek terrane in northwestern British Columbia preserves aerially extensive ophiolites, but few detailed petrological and geochemical studies of these rocks have been carried out, despite their importance to tectonic models of the Cordillera (Terry 1977, Ash and Arksey 1990, Ash 1994, Canil et al. 2006). Herein we build on work by English et al. (2010) in the northern Cache Creek terrane, which identified two distinct magma suites in this region: abundant subalkaline plutonic and volcanic rocks with arc signatures, and minor alkaline within-plate volcanic rocks, an association also noted in central British Columbia (Tardy et al. 2001, Lapierre et al. 2003). The close spatial association of volcanic rocks originating in two different plate settings has implications for the emplacement of the Nahlin ophiolite, and models involving closure of ocean basin for Cache Creek terrane accretion, and overall continental growth in the northern Cordillera.

In this contribution, we investigate the geological relationships and petrochemistry of the Nahlin ophiolite and adjacent rocks in the Menatatuline Range area of northern British Columbia. The Nahlin ophiolite is the largest, best-preserved and well-exposed ophiolite in the Cache Creek terrane (**Figure 1**; **Table 1**), however, due to its remote location it has not been investigated in detail since Terry (1977). We present new field and lithogeochemical data constraining the relationships between mantle, lower crustal and supracrustal rocks in the Nahlin ophiolite, and the spatial connection to accreted alkaline basalt and carbonate platform sequence.

Regional Geology

The Mississippian to Lower Jurassic Cache Creek terrane is discontinuously exposed through British Columbia and southern Yukon and is bound by the peri-Laurentian Yukon-Tanana, Quesnellia and Stikinia terranes. Permian carbonate rocks of the Cache Creek terrane contain Tethyan fauna that is distinct from that in adjacent Stikinia and Quesnellia, indicating

that parts of the Cache Creek terrane are exotic with respect to Laurentia and adjacent terranes (Monger and Ross 1971, Orchard et al. 2001). The Cache Creek and adjacent terranes were amalgamated and stitched together by crosscutting plutons by the Middle Jurassic (Gabrielse 1991, Mihalynuk et al. 1992, 1998). The aforementioned contrasting faunal assemblages between the accreted terranes has strongly influenced tectonic models for the northern Cordillera (e.g., Mihalynuk et al. 1994, Johnston and Borel 2007). Although central to several such models, the tectono-stratigraphy and tectonic setting of the Cache Creek terrane remain poorly understood. Some authors treat the whole or parts of the Cache Creek terrane as a subduction zone melange or an accretionary complex (e.g., Mihalynuk et al. 1994, 2004b, Mihalynuk 1999, English and Johnston 2005, English et al. 2010).

The geology of northern Cache Creek terrane near Atlin, BC and extending southeast to the Menatatuline Range has been the focus of several studies that are mostly regional in scope (e.g., Aitken 1959, Souther 1971, Monger 1975, Terry 1977, Bloodgood and Bellefontaine 1990, Ash 1994, Mihalynuk et al. 1994). Varied interpretations based on these studies suggest that the Cache Creek terrane in this region comprises several distinct and possibly unrelated components including: an ophiolite and/or rifted arc (e.g., Childe and Thompson 1997, English et al. 2010, Bickerton et al. 2012, Schiarizza 2012), seamounts and/or oceanic plateaus (e.g., English et al. 2010), and a subduction-related accretionary complex (Monger 1975, Terry 1977, Ash 1994, Mihalynuk et al. 1998, English and Johnston 2005).

Geology of the Menatatuline Range area

The Nahlin ophiolite was first recognized in this region by Aitken (1959). Recent geochronological data indicate a regional age variation of magmatism in the Nahlin ophiolite of 261 to 245 Ma (**Figure 1**; **Table 1**). A summary of the geology of the ophiolite is presented

below. Detailed descriptions of all the lithological units within the Menatatuline Range area are presented elsewhere (Zagorevski et al. 2015, 2016a, McGoldrick et al. 2016).

Ultramafic rocks in the Nahlin ophiolite

The best exposures of ultramafic rocks occur in a discontinuous belt from Atlin townsite to Nahlin Mountain about 150 km southeast (**Figure 1**). For convenience we herein subdivide the Nahlin ophiolite into the Atlin, Hardluck, and Menatatuline massifs. The Menatatuline massif trends northwest from Nahlin Mountain through the Menatatuline Range (Aitken 1959, Terry 1977). The Hardluck massif trends west-northwest from the Menatatuline (**Figure 2**; Mihalynuk et al. 2004b).

Ultramafic rocks in both the Hardluck and Menatatuline massifs comprise variably serpentinized harzburgite (0 – 50%) with pyroxenite dikes, and replacive dunite pods (McGoldrick et al. 2016). Massive and layered harzburgite is the dominant lithology and contains ~45-65% olivine, ~25-40% orthopyroxene, 3-8% clinopyroxene, and <5% spinel. Layering defined by modal variation of pyroxene is variably developed in both massifs. Lherzolite with up to 15% emerald-green clinopyroxene occurs in the Hardluck massif (Mihalynuk et al. 2004b). A primary mantle tectonite fabric (S_1) defined by orthopyroxene porphyroclasts is variably developed in both massifs. Pyroxenite dikes (5–10 cm wide) are variably abundant. In both the Hardluck and Menatatuline massifs, pyroxenite dikes can be layer-discordant or concordant with respect to the harzburgite layering (**Figure 3a**). Dikes are locally deformed into meter-scale folds (**Figure 3b**) and rarely cut folded harzburgite-pyroxenite layering. Discrete dunite pods comprise as much as 20% of the Menatatuline and Hardluck massifs. The size of individual pods is variable, ranging from sub-metre scale up to 100 m across. Dunite bodies have sharp contacts against harzburgite, are locally deformed and crosscut

pyroxenite, indicating that there are several generations of these features. The dunite likely represents melt channels formed as a result of melt-rock interaction with the host harzburgite (Kelemen and Dick 1995).

Cumulates

Mafic-ultramafic cumulates are rare in the Nahlin ophiolite and have only been documented in few localities (Terry 1977, Gabrielse 1998, Mihalynuk et al. 2004b, Zagorevski et al. 2016b). Minor cumulates have been documented in the Hardluck massif northwest of the study area ("Moho Saddle", **Figure 1**; Mihalynuk et al. 2004b). Pods of pyroxenitic to gabbroic cumulates intrude variably serpentinized harzburgite on the southern margin of the Hardluck massif in the Tseta Creek area (**Figure 2**). Some pods have highly irregular scalloped margins against the host harzburgite suggesting high temperature, ductile deformation within the lithosphere (**Figure 4a**). Cumulates include varitextured plagioclase-bearing olivine websterite and gabbronorite, that vary in grain size from fine grained to pegmatitic over meters. Granoblastic textures and primary mineralogy are variably overprinted by green amphibole, chlorite, serpentine, sericite and/or prehnite.

Gabbroic rocks

Fine grained to pegmatitic gabbros (plagioclase- pyroxene ± amphibole) intrude the harzburgite tectonite along the southern margin of the Hardluck massif, and throughout the Menatatuline massif. In the Hardluck massif, gabbroic dikes and pods with chilled margins commonly intrude serpentinite, most notably north of the Nahlin fault near Peridotite Peak (**Figure 4b**). Foliated amphibole- and plagioclase-rich zones are locally present in the gabbro. Gabbro becomes less abundant toward the north, where it typically forms thin dikes ± sills and reticulated dike and vein swarms within variably serpentinized peridotite. It is unclear whether

these gabbroic intrusions exclusively represent dikes, sills, or a combination of both, as their original orientation within the mantle is ambiguous. Some exposures of gabbro are completely enveloped within fresh peridotite.

Gabbroic dikes ± sills ranging in width from <2 to 20 m occur as a west- to north-trending swarm crosscutting the Menatatuline massif. Some are undeformed (**Figure 4c**), whereas others are boudinaged (**Figure 4d**). Dike cores typically comprise fine to medium grained equigranular plagioclase (40–50%) and pyroxene (1–3 mm). Many of these dikes display subophitic to intergranular textures, and are variably plagioclase ± clinopyroxene ± orthopyroxene-phyric (<5%, 2-4 mm phenocrysts). Some dikes have chilled margins against the host harzburgite. Primary mafic mineralogy, including sparse igneous amphibole, is variably altered to lower greenschist facies assemblages of chlorite + epidote ± actinolite ± sericite.

Nahlin ophiolite volcanic and volcaniclastic rocks

Volcanic and volcaniclastic rocks are aerially extensive in the northern Cache Creek terrane. Some of these rocks were previously mapped as the Nakina Formation (Monger 1977, Mihalynuk et al. 1996, 2002, English et al. 2002), although this stratigraphic name was originally defined only for Mississippian – Permian volcanic rocks associated with carbonate successions (Monger 1975). Here we avoid this nomenclature to prevent confusion.

Brecciated, massive and rare pillowed flows, with locally pervasive chlorite ± hematite alteration are exposed northeast of the Menatatuline massif, and between it and Hardluck massif (**Figure 2**). Younging directions and contact relationships within these sequences are unclear. The mafic volcanic rocks are plagioclase, clinopyroxene, and orthopyroxene porphyritic. Some plagioclase phenocrysts display sieve textures and growth zoning. Flows are locally highly

158 vesicular, with calcite ± chlorite-filled amygdules. Primary mafic minerals are variably altered to
159 chlorite ± actinolite (clinopyroxene), and to chlorite + calcite ± epidote ± sericite (plagioclase).

160 The volcaniclastic rocks comprise mafic crystal and lapilli tuffs that are fine grained,
161 locally vesicular and flow banded. Lapilli and crystal fragments are rounded to subangular, and
162 rarely elongate or shard-like (**Figure 5**). Crystal fragments comprise plagioclase ± orthopyroxene
163 ± clinopyroxene, and one sample contains serpentine pseudomorphs of equant olivine
164 phenocrysts. Lapilli fragments in the pervasively chloritized ± hematized groundmass preserve
165 volcanic textures, such as intergranular and pseudotrachytic groundmass textures, to varying
166 degrees.

167 **Geochemistry**

168 ***Methods***

169 Representative samples of all the lithologies described above were selected for
170 lithogeochemical analysis to constrain the petrogenesis of the igneous rocks in the Nahlin
171 ophiolite. The major, minor, and trace element data presented herein are from 28 samples of
172 intrusive and extrusive rocks. A more detailed study of the harzburgite tectonite will be
173 presented elsewhere. Samples were cut into slabs with a rock saw, and were crushed and
174 processed for bulk rock geochemistry at Activation Laboratories in Ancaster, Ontario (**Table 2**).
175 Major oxides were measured by lithium metaborate/tetreborate fusion and ICP-OES, whereas
176 minor and trace elements were determined by ICP-MS. The suite of standards analysed along
177 with the samples reproduce reported concentrations of major elements to within 9%, large-ion
178 lithophile elements (LILE) to within 13%, high-field strength elements (HFSE) to within 9%,
179 and rare-earth elements (REE) to within 7% (**Table 2**).

Element Mobility

All the samples have experienced up to greenschist facies metamorphism, which can result in element mobility. Elements such as Ti, Zr, Hf, Nb, and Ta, and the REE have been shown to be relatively immobile during hydrothermal alteration and up to greenschist facies metamorphism (MacLean 1990, Jenner 1996, Pearce 1996). Using discriminant diagrams involving the immobile elements Nb, Y, Zr and Ti, the vast majority of the intrusive, volcanic, and volcaniclastic samples of the Menatatuline Range area classify as subalkaline, and basaltic to basaltic andesite (**Figure 6a**). An identical result is obtained for these rocks using the more traditional alkalies-silica classification scheme **(Figure 6b)**, showing Na and K have not been compromised by metamorphism. Molecular proportion diagrams (**Figure 7**), which compare the composition of the whole rocks with the stoichiometry of minerals involved in their differentiation, suggest that most major elements (Na, K, Si, Mg, Fe, Ca) were largely unaffected by metamorphism. For example, with the exception of two samples, the gabbros, dikes and mafic volcanic rocks lie along tielines between plagioclase, clinopyroxene and olivine components (Figure 7), a trend that is predicted during low-pressure crystallization of basaltic magma.

Basalts and gabbro dikes

Most of the basalts and gabbros of the Menatatuline Range area are subalkaline and basaltic in terms of major and trace elements (**Figure 6**). These rocks lie along differentiation trends consistent with accumulation or removal of plagioclase and clinopyroxene (CPX – $CaMgSi_2O_6$, CaTs - $CaAl_2SiO_6$), as observed petrographically in the rocks **(Figure 7)**. Many of the samples are similar to the reference N-MORB composition (grey triangle, **Figure 6a**), and major and trace element data indicate that these rocks are predominantly tholeiitic (**Figure 6, 8**). Ratios of Nb/Yb indicate that the volcanic and plutonic samples from the Nahlin ophiolite plot

near reference values for N-MORB (**Figure 9**), suggesting derivation from a depleted source. However, many of the Nahlin ophiolite rocks also show variable enrichment of Th/Nb over N-MORB, and plot along the subduction enrichment trend. On N-MORB normalized trace element plots, the volcanic and plutonic rocks of the Nahlin ophiolite have similar flat trace element profiles displaying consistent negative Nb-anomaly (**Figure 10**).

A narrow unit of distinctly more enriched volcanic rocks also occurs in the Menatatuline Range area (**Figure 2**). These are subalkaline basalts with higher Nb/Y ratios than the majority of the volcanic rocks of the ophiolite and close to the reference value for E-MORB (**Figure 6b**; Sun and McDonough 1989). Trace element data indicate that these volcanic rocks are tholeiitic to transitional (**Figure 8**). Other trace element ratios indicate that these samples have E-MORB-like chemistry, and plot along the source enrichment trend between reference compositions for N-MORB (depleted source) and OIB (enriched source) (**Figure 9**). The E-MORB-like volcanic rocks lack the subduction enrichment of Th/Nb recorded in the volcanic rocks of the ophiolite (**Figure 9**). Multi-element diagrams highlight the enrichment of LREE over HREE, and lack of Th-Nb and Ti anomalies in these samples (**Figure 10**).

A series highly vesicular basalts are petrographically and geochemically distinct from the other basalts of the ophiolite in the field. These rocks contain serpentine pseudomorphs after subhedral to euhedral 0.5 to 1 mm olivine phenocrysts, sparse subhedral to euhedral 1-4 mm plagioclase phenocrysts which are variably altered to sericite + calcite, and up to 30% calcite-filled amygdules that are typically 1 mm in diameter. These highly vesicular basalts plot along an olivine control line (Figure 7ab) consistent with olivine accumulation observed petrographically. Two samples of these mafic volcanic rocks lack Nb anomalies, have significant enrichment in

LREE over HREE, and Nb/Y typical of alkali basalts (**Figures 6, 9, and 10**) such as typical ocean island basalt (OIB; Sun and McDonough 1989).

Ultramafic and mafic cumulates

The major element composition of the cumulates lie along tielines between either olivine, clinopyroxene or plagioclase – all phases observed to vary modally in these rocks (Figure 7). Some of the trace element diagrams employed above to characterize the volcanic and plutonic rocks are inappropriate for cumulates (Langmuir 1989, Bédard 1994, Pearce 1996). Multi-element plots, however, can still be useful in the petrogenetic interpretation of these non-liquidus compositions (Bédard 1994). The plagioclase-bearing olivine websterite and gabbronorite cumulates have flat trace element profiles nearly an order of magnitude more depleted than the other intrusive rocks of the ophiolite (**Figure 10**). The plagioclase-bearing olivine websterite has a pronounced negative Eu anomaly, whereas the gabbroic cumulates show slight positive Eu anomalies, reflecting variable fractionation and accumulation of plagioclase. All the cumulate samples are enriched in Th ± Nb relative to the REE, but lack the negative Nb anomalies characteristic of other plutonic rocks of the ophiolite (**Figure 10**).

Discussion

Stratigraphy and structure of the Nahlin ophiolite

The Nahlin ophiolite contains some components of the classic Penrose-style ophiolite (Anonymous 1972) , and though some primary contact relations may be obscured by faulting, it is still possible to constrain the stratigraphy of the ophiolite (**Figure 11**). The harzburgite massifs at the base of the Nahlin ophiolite are interpreted as mantle lithosphere and are locally crosscut by multiple generations of gabbroic dikes, some of which are unstrained (**Figure 4c**) whereas

247 others have been boudinaged within the mantle (**Figure 4d**). Lower crustal cumulates and
248 sheeted dike complexes are volumetrically minor in the Nahlin ophiolite. Locally, gabbroic dike-
249 and-sill complexes extensively intrude the mantle rocks. These melt conduits presumably fed
250 volcanic flows at the surface, which are represented by the aerially-extensive basalt and related
251 mafic volcaniclastic rocks in the Menatatuline Range area (in part formerly mapped as Nakina
252 Formation). Some of these massive mafic rocks have previously been mapped as volcanic flows,
253 even where they lack any extrusive textures (Gabrielse 1998, Mihalynuk 1999, Mihalynuk et al.
254 2003) but are now recognized as hypabyssal dike-and-sill and sill-sediment complexes
255 (Zagorevski et al. 2016a).

256 Constraining the stratigraphic way-up in the Nahlin ophiolite is not everywhere
257 straightforward. A section through the uppermost mantle and into the lowermost crust is exposed
258 at the "Moho Saddle" (**Figure 2**) to the northwest of Peridotite Peak, and indicates that the
259 ophiolite youngs towards the south (Mihalynuk et al. 2004b). The presence of rare pyroxenitic
260 and gabbroic cumulates exclusively on the southern side of the Hardluck massif supports this
261 interpretation. Elsewhere in the Nahlin ophiolite, however, the harzburgite massifs are fault-
262 bound, leaving little evidence as to the way-up in stratigraphy. These fault-bound sections of
263 mantle harzburgite tectonite are often juxtaposed against basalt or chert. A possible interpretation
264 for this juxtaposition and the locally missing lower crustal section, is that the Nahlin ophiolite
265 represents an intraoceanic core complex (Zagorevski et al. 2015). Similar to other fossil oceanic
266 core complexes recognized in the rock record (e.g., Ohara et al. 2003, Maffione et al. 2013,
267 Lagabrielle et al. 2015), the spinel-facies harzburgite tectonite may have been exhumed along a
268 low angle normal fault to shallow depths (plagioclase stability zone), where it acted as a rigid
269 body during the intrusion of later gabbroic dikes.

Tectonic setting of the Nahlin ophiolite

The reconstructed stratigraphy of the Nahlin ophiolite based on recent field work in the northern Cache Creek terrane can be corroborated using lithogeochemical data. The gabbro and diabase dikes that crosscut the mantle sections of the Nahlin ophiolite have arc tholeiitic chemistry, and REE profiles identical to those of spatially associated basalt and mafic volcaniclastic rocks (**Figure 10**). The flat to low positive slope of the REE profiles (**Figure 12**), and the low Nb/Yb ratios, indicate derivation from a LREE-depleted mantle source that experienced earlier melt extraction (Jenner 1996, Pearce 1996). The intrusive and extrusive rocks are enriched in Th/Yb over typical N-MORB values (**Figure 9**), suggesting that subduction-related fluids played a role in the genesis of the ophiolite crust. All of the plutonic and volcanic rocks display a negative Th-Nb-La anomaly (**Figure 10**) and enrichment of LILE over HFSE. These characteristics are generally considered a subduction zone signature similar to that of island arc tholeiites (IAT), and are linked to relative contributions of these elements from the subducting slab to the source of the arc magmas (Pearce and Norry 1979, Saunders et al. 1988, Pearce and Peate 1995, Jenner 1996, Pearce 1996). The remarkably consistent arc tholeiite chemistry, subduction-related enrichment, and the crosscutting relationships linking the gabbroic rocks to the mantle suggest that the Hardluck and Menatatuline massifs are part of a supra-subduction zone (SSZ) ophiolite.

Rare earth element profiles of the extrusive igneous rocks in the Nahlin ophiolite can be compared to melt compositions produced by fractional melting of peridotite, to constrain the degree of melting required to generate the crust of the Nahlin ophiolite. Melting models employed in this study follow the methodology of Warren (2016), in which a depleted MORB mantle (DMM) source (Workman and Hart 2005) undergoes non-modal fractional melting in the

spinel stability field according to the melting reaction 0.56 Opx + 0.72 Cpx + 0.04 Sp = 0.34 Ol + 1.0 Melt (Wasylenki et al. 2003). Partition coefficients melt for the REE are after Sun and Liang (2014) and Warren (2016), and are calculated assuming a mantle of DMM composition at a potential temperature of 1300 °C. The range of REE profiles of the Nahlin ophiolite basaltic rocks is reproduced by 2 to 20% non-modal fractional melting (**Figure 12**). This suggests that some of the volcanic rocks represent erupted products of low degrees of partial melting, whereas others result from combined segregated melts of up to 20% melting. Considering the range of MgO values (~4 to 9 wt %; **Table 2**), we assume that most of these volcanic rocks do not represent primary or primitive melts (Niu and Batiza 1991, Kinzler and Grove 1992). The REE in basalt will increase in abundance with crystal fractionation of early olivine. In this way the concentrations of REE in Nahlin arc tholeiites are higher than in their original primitive parental melts, requiring that our melt fraction estimates are minima.

The mantle melting model described above also provides a residual mantle composition, which can be compared to peridotites of the Nahlin ophiolite. Whole-rock REE data from peridotite samples near the "Moho Saddle", Peridotite Peak, and Peridotite Peak East (Babechuk et al. 2010) require 10 to 20% partial melting to reproduce measured HREE concentrations (**Figure 12**). Light REE enrichment of the Nahlin peridotites is not predicted by the modeled residue compositions, but may be related to cryptic mantle metasomatism or refertilization that is observed in many abyssal and ophiolite peridotites (e.g., Bizimis et al. 2000, Warren and Shimizu 2010, Uysal et al. 2016). The range of melt depletion recorded in the peridotites (10 – 20 %) overlaps with the melt estimates necessary to generate the basaltic rocks of the Nahlin ophiolite (2 – 20 %). This indicates that the arc tholeiite intrusive and extrusive igneous rocks in the Menatatuline Range area are demonstrably the products of the Nahlin harzburgites with

316 which they are spatially associated. Alternatively, the arc tholeiite magmatism in the Nahlin
317 ophiolite was established on mantle lithosphere that experienced previous history of arc
318 magmatism. Geochronological constraints on the timing of volcanism are needed to discriminate
319 between these hypotheses. Regardless, the mantle harzburgites of the Nahlin ophiolite are thus
320 not related to the OIB and E-MORB sequences.

321 ***Connection to other Cache Creek assemblages***

322 Tholeiitic plutonic and volcanic rocks of the Nahlin ophiolite display a predominantly
323 arc-backarc geochemical signature. A similar arc-backarc setting has been inferred along-strike
324 to the north in the Nakina area (English et al. 2010), and to the south in the Kutcho assemblage
325 (Childe and Thompson 1997, Mihalynuk and Cordey 1997) (**Figure 1**). The oceanic crustal
326 assemblage in the Nakina area (**Figure 1**) (English et al. (2010) comprises Middle to Late
327 Permian intrusive and extrusive igneous rocks of variable affinity (e.g., IAT, backarc basin basalt
328 (BABB), calc-alkaline) that formed from a depleted N-MORB-like source in an arc or backarc
329 setting (Devine 2002, English et al. 2010). As these rocks are physically continuous with and
330 chemically similar to those in the Nahlin area, they could form part of the same arc-backarc
331 system as the Nahlin ophiolite (**Figure 10**).

332 The Early to Middle Triassic Kutcho arc exposed near Dease Lake (**Figure 1**) was
333 previously correlated with the Nakina area (English and Johnston 2005, English et al. 2010). The
334 Kutcho assemblage is characterized by bimodal tholeiitic volcanic and volcaniclastic rocks that
335 formed in a intra-oceanic arc (ca. 254-242 Ma: (Barrett et al. 1996, Childe and Thompson 1997,
336 Barrett and MacLean 1999, Schiarizza 2012). The Kutcho assemblage and the Nahlin ophiolite
337 likely represent different segments of the same, extensional Late Permian to Middle Triassic arc-
338 backarc system, similar to the modern Izu-Bonin-Mariana or Tonga-Tofua-Kermadec arcs

(Reagan et al. 2010, 2013, Ishizuka et al. 2011 ; Smith and Price 2006)). In such analogues, the Nahlin ophiolite could represent more advanced stages of rifting, similar to the Lau and Parece-Vela basins, whereas the Kutcho assemblage either represents an incipient rift or highly extended arc (e.g., southern termination of west Mariana Trough or parts of the of the Lau basin).

Alternatively, the Kutcho assemblage and Nahlin ophiolite may represent along strike variations in magmatic versus tectonic-accommodated extension in the backarc region, and in the nature of the slab derived components added to the mantle wedge as described in the southern Havre Trough (Wysoczanski et al. 2010, Todd et al. 2011). This configuration reflects anomalous thermal regimes in the mantle wedge ("hot fingers", Tamura et al. 2002, Todd et al. 2011) which result in cross-arc chains of constructive volcanic centres separated by basinal 'rift regimes' in which BABB are erupted (Wysoczanski et al. 2010). Application of such a setting to the northern Cache Creek composite terrane can explain the apparent lack of a mature Permo-Triassic arc spatially associated with the Nahlin ophiolite (**Figure 13**).

Alternatively, the Nahlin ophiolite may have formed in a proto-forearc setting associated with subduction initiation. Similar to the proposed origin of the Izu-Bonin-Mariana arc, nucleation of a new intraoceanic subduction zone may have been accompanied by seafloor spreading in what would become the forearc region (**Figure 13**; Stern et al. 2012, Maffione et al. 2015). A progressive change in volcanic chemistry from initial forearc spreading to development of a mature arc follows from the evolution of tholeiitic MORB-like volcanic rocks (forearc basalts) at the base to volcanic arc-like basalts including boninites at the top of the volcanic sequence in the forearc (Reagan et al. 2010, 2013, Ishizuka et al. 2011, Stern et al. 2012). This chemostratigraphy is recognized in other SSZ ophiolites (Mirdita and Pindos ophiolites - (Saccani and Photiades 2004, Dilek et al. 2008, Whattam and Stern 2011), but is not recognized

in the Nahlin ophiolite, perhaps due to structural dismemberment. A subduction initiation origin may also account for the lack of a preserved arc associated with the Nahlin ophiolite, as a newly nucleated convergent margin may be short-lived and need not develop a mature arc (Whattam and Stern 2011).

The relevance of OIB and E-MORB

The two E-MORB-type volcanic rocks in the Menatatuline Range area define a thin belt along the contact of the volcanic rocks of the ophiolite and the Kedahda Formation (**Figure 2**). Enriched MORB-like basalts have been described to the north in the Nakina area (English et al. 2010). These volcanic rocks require an enriched non-arc source indicating that these rocks cannot be directly related to the arc tholeiites of the Nahlin ophiolite. The volumetrically minor E-MORB magmatism could represent continued spreading in the backarc environment and tapping of a more enriched mantle source or it may reflect a heterogeneous mantle source that includes both depleted and enriched components (e.g., Pomonis et al. 2006, Dilek and Furnes 2009, Gale et al. 2013, Wilson et al. 2013). Alternatively, the E-MORB-type volcanic rocks may be unrelated to the ophiolite. The complete lack of any subduction zone signature, and the proximity of these basalts to a fault imbricated package of siliciclastic, chert and carbonate rocks, may indicate that the E-MORB-type samples are a part of the Tethyan carbonate successions.

Non-arc magmatism is well-documented elsewhere in the northern Cache Creek terrane. For example, the Teslin Formation limestone with its Permian Tethyan fauna is stratigraphically intercalated with French Range Formation E-MORB-type basalt and related felsic volcanic rocks which yielded a ca. 263 Ma U-Pb zircon crystallization age (Monger 1975, Mihalynuk and Cordey 1997, English et al. 2010). Permian Teslin Formation limestone in the Hall Lake area is also intercalated with OIB (Monger 1975, Mihalynuk and Cordey 1997). Carboniferous OIB and

385 related rhyolite is also known to occur within the Horsefeed Formation limestone (Devine 2002,
386 Merran 2002).

387 The intraplate (OIB) volcanic rocks and their associated carbonate platforms have been
388 proposed to represent fragments of exotic oceanic plateaux or seamounts (Monger 1975, English
389 et al. 2010). These successions were likely sheared off the down-going plate and accreted to the
390 Late Permian to Early Triassic arc which is, in part, represented by the Nahlin ophiolite (c.f.
391 English et al. 2010). Incorporation of the E-MORB-OIB-carbonate platform sequences in to the
392 subduction channel is supported by local preservation of blueschist-facies metamorphism in the
393 French Range Formation (Mihalynuk et al. 1998).

394 ***Significance to Cordilleran tectonic models***

395 Field and lithogeochemical data indicate that mantle, lower crustal and supracrustal rocks
396 of the Nahlin ophiolite formed within a Permo-Triassic arc system. Rocks of the ophiolite in
397 northern Cache Creek terrane were previously grouped with the intraplate volcanic rocks,and
398 Tethyan carbonate successions, as part of the subducting slab of the Cache Creek ocean basin
399 (e.g., Ash, 1994; Monger 1975, 1977, Mihalynuk et al. 1992, 1994, 1999, 2004a, Nelson and
400 Colpron 2007). But the preservation potential of large tracts of ophiolite that forms part of the
401 subducting plate is poor, because subducting lithosphere lacks the buoyancy to cause orogenesis
402 (Cloos 1993). Furthermore, the accreted ophiolites are typically small and lack lower crust and
403 mantle sections (Kimura and Ludden 1995, Zagorevski et al. 2009, Zagorevski and van Staal
404 2011). In contrast, the herein proposed arc-backarc setting of the Nahlin ophiolite has a greater
405 preservation potential and is consistent with the occurrence of an extensive mantle section, which
406 is characteristic of obducted ophiolites (Zagorevski and van Staal 2011). The Nahlin ophiolite
407 thus represents the upper plate at an intraoceanic convergent margin. The structurally-imbricated

Mississippian to Permian limestone, alkaline volcanic rocks and chert, including those that are characterized by Tethyan fauna, must represent part of the subducting ocean basin. This view is supported by preservation of blueschist in the nearby French Range (Mihalynuk et al. 1998).

The regional map patterns in the northern Cache Creek composite terrane are complicated by overprinting by deformation episodes including poorly exposed obduction structures, Jurassic E-W trending folds and thrust faults, and northwest trending Cretaceous strike-slip faults. The ophiolite is generally exposed to the southwest of the 'Cache Creek Complex' (the subduction accretionary complex including OIB-carbonate successions, English et al. 2010). This distribution suggests that the ophiolite was obducted along northeast-vergent structures over a southwest dipping intraoceanic subduction zone (cf. English et al 2010).

Nonetheless, the upper and lower plate domains we identify herein (**Figure 11**) represent fundamentally different associations of rocks, and therefore meet the definition of two separate "terranes" : fault-bound areas possessing unique tectonic assemblages that differ from those of adjacent terranes (Gabrielse et al. 1991). The true terrane-bounding fault in the northern Cache Creek terrane is not, therefore, the Nahlin fault **Figure 1**), but rather the suture between the upper and lower plate assemblages, where it is exposed. Contrary to the current terrane boundaries, this suture cannot be neatly drawn as an orogen near-parallel fault, but its approximate equivalents can be observed in outcrop. At Mount Nimbus (**Figure 1**), for example, ophiolite is thrust over Mississippian carbonate successions bearing OIB-type volcanic rocks (Zagorevski et al. 2016a).

The proposed separation of the composite Cache Creek terrane into arc and seamount terranes has significant implications for the interpretation of oceanic terranes in the Cordillera, including the Cache Creek composite terrane further south, where grouping of overriding and

subducting plates into a single terrane results in significant misadventure. For example, the presence of OIB, E-MORB and N-MORB-like basalts in the Cache Creek terrane near Fort St. James led to a suggestion for its formation in a ridge-centered or near-ridge oceanic island plateau environment (Tardy et al. 2001, Lapierre et al. 2003). Some of the Cache Creek MORB-like samples of Lapierre et al. (2003; Type 1 N-MORB) actually show significant negative Nb anomalies indicating that these samples are likely island arc tholeiites and are not related to alkaline lavas at all. Their association with gabbroic and harzburgitic rocks suggest that, together with the mantle harzburgite, the basalts are correlative to the Nahlin ophiolite, consistent with their inferred age (ca. 257 Ma; Struik et al. 2001). These rocks also lie adjacent to the Sitlika Assemblage (Childe and Schiarizza 1997), a correlative of the Kutcho Assemblage. Following our proposed tectono-stratigraphic relationships for the northern Cache Creek terrane, the alkaline and E-MORB volcanic rocks and associated carbonates in Fort St. James area form part of the lower, partly subducted plate onto which the Trembleur ophiolite and Kutcho - Sitlika arc rocks were obducted.

Conclusions

Intrusive and extrusive igneous rocks of the Nahlin ophiolite in the northern Cache Creek composite terrane are dominantly subalkaline and of arc-affinity. The arc tholeiites represent the products of up to 20% partial melting, and are the melt complement to similar levels of melting recorded by harzburgite residues in the mantle section of the ophiolite. The volcanic rocks of the Nahlin ophiolite are likely correlative to the nearby subalkaline volcanic rocks in the Nakina transect and Kutcho assemblage, and may be linked to a regionally extensive Permo-Triassic intraoceanic arc. During the amalgamation of the composite Cache Creek terrane, this arc occupied the upper plate thereby facilitating the preservation of extensive fragments of oceanic

lithospheric mantle. The volumetrically minor OIB-type volcanic rocks associated with Tethyan fauna-bearing carbonate successions represent fragments of oceanic plateaux and their carbonate atolls sliced off of the subducting plate and incorporated into a subduction accretionary complex. These sequences are older than and petrogenetically unrelated to the Nahlin ophiolite. This configuration challenges some accepted models for the Cache Creek terrane and the terrane-bounding Nahlin fault. A re-evaluation of terrane-bounding structures in this light is paramount to a better understanding of the assembly and displacement of terranes in the northern Cordillera.

Acknowledgments

The authors thank N. Graham and P. Vera at Discovery Helicopters Ltd. Atlin B.C. for reliable transport. We are grateful to R. Maxeiner and R. Stern for their reviews. This research was supported by the Geological Survey of Canada's Geomapping for Energy and Minerals program (GEM2-Cordillera), Natural Sciences and Engineering Research Council of Canada (NSERC) and Geoscience BC scholarships (S. McGoldrick), and NSERC Discovery grant (D. Canil).

Figure Captions

Figure 1: Lower inset map shows terranes of northern British Columbia and Yukon highlighting the Cache Creek terrane (CC; yellow) and location of the Menatatuline Range study area (red star). Main panel shows the regional geology of the northern Cache Creek composite terrane in Yukon and British Columbia. The Menatatuline Range study area is outlined in red dashed lines. Other localities referenced in text include: Nakina transect (NK, black dashed box), Hall Lake (HL), "Moho Saddle" (MS), Mount Nimbus (MN), French Range (FR), and the Kutcho assemblage (KT). Diamonds refer to locations of geochronological data in Table 1. Inset map modified after Nelson and Colpron (2011). Main panel map modified after Zagorevski et al. (2015).

Figure 2: Bedrock geology of the Menatatuline Range area, from Peridotite Peak to Nahlin Mountain, based on 2015 – 2016 mapping and compiled from previous data of Mihalynuk et al. (1996). Sample locations symbolized by lithology and chemical affinity as discussed in text. Names of geological features referenced in text are in italic font (e.g. Nahlin fault). Informal place names are indicated by quotation marks (e.g., "Tseta Creek area"). Background topographic raster image from Natural Resources Canada (1990a, 1990b).

Figure 3: Field pictures of ultramafic rocks of the Nahlin ophiolite. (A) Primary tectonic fabric (S_1), and pyroxenite dike transposed into S_1, in harzburgite tectonite truncated by a replacive dunite pod on Peridotite Peak. (B) Tight, near isoclinal folding of a pyroxenite dike in harzburgite tectonite on Peridotite Peak.

Figure 4: Field images of intrusive rocks of the Nahlin ophiolite in the Menatatuline Range area. **(A)** Boudinaged altered ultramafic cumulate (pale) with scalloped margins surrounded by

harzburgite (dun brown), on the southern side of the Hardluck massif. **(B)** Varitextured gabbro intrusion on the southern side of the Hardluck massif. Grain size within the gabbroic intrusions can vary from fine grained (top) to pegmatitic (bottom) for the sample shown. **(C)** Planar margins (white dashed lines) of a gabbroic dike intruding harzburgite at Nahlin Mountain. **(D)** Boudinaged gabbroic dikes protruding along the slopes of Nahlin Mountain among recessively weathering serpentinite scree.

Figure 5: Images of mafic volcanic rocks previously grouped as part of the Nakina Formation, in northwestern British Columbia. **(A)** Locally fragmental texture in pervasively hematized volcaniclastic rocks. **(B)** Photomicrograph of an ultramafic crystal tuff with orthopyroxene crystal fragments, and serpentine pseudomorphs after rounded olivine fragments in PPL, and **(C)** in XPL. **(D)** Photomicrograph of a mafic tuff with lapilli in PPL, and **(E)** in XPL.

Figure 6: Igneous rock discrimination diagrams using **(A)** trace element ratios (Pearce 1996) and (B) SiO_2 versus total alkalis (Le Maitre 1989). The mafic volcanic rocks, gabbros, and gabbroic dikes of the Nahlin ophiolite are all subalkaline and basaltic to andesitic in composition, with the exception of one gabbro, which may have experienced enrichment in alkalis. One of the alkali basalts (blue circles) plots within the subalkaline basalt field, suggesting it may have experienced variable degrees of silicification and/or alkali loss. Reference composition for normal mid-ocean ridge basalt (N-MORB), enriched mid-ocean ridge basalt (E-MORB), and ocean island basalt (OIB) shown in grey symbols for comparison (Sun and McDonough 1989). Data from igneous rocks of the Nakina transect shown for comparison (black crosses; English et al. 2010).

Figure 7: Covariation of molar (a) Na+K, (b) Ca+Na and (c) Mg+Fe with Si+Al in the intrusive and extrusive rocks of the Menatatuline range area (this study) as well as other literature data for the Nakina region in northern Cache Creek terrane (English et al, 2010). Plotting in molar space shows the mineral stoichiometric control on bulk rock compositions. Note the trend of the intrusive and extrusive mafic rocks along control lines (dashed) between clinopyroxene components (CPX, CaTs) and plagioclase (PL), and of the olvine-phyric alkali basalts and cumulate rocks toward olivine (OL). CPX, clinopyroxene; CaTs - Ca-tschermaks pyroxene; OL, olivine; PL, plagioclase.

Figure 8: Discrimination of magma series by trace element data following the method of Ross and Bédard (2009). The rocks of the ophiolite are predominantly tholeiitic. Volcanic rocks from the southern Cache Creek terrane shown for comparison with northern Cache Creek data (black "x" symbols; Tardy et al. 2001, Lapierre et al. 2003). All other symbols as in Figure 6.

Figure 9: Lithogeochemical data for samples from the northern Cache Creek terrane plotted in Nb/Yb – Th/Yb space. Reference compositions for N-MORB, E-MORB, and OIB are shown for comparison (grey symbols; Sun and McDonough 1989). Samples derived from an enriched source plot near the OIB reference point with high Th/Yb and Nb/Yb ratios. The majority of the Nahlin ophiolite samples of both plutonic and volcanic rocks plot near the N-MORB reference value, but show evidence of subduction-related enrichment. Data from the Nakina Transect (English et al. 2010), and from volcanic rocks in the southern Cache Creek terrane in central BC (Tardy et al. 2001, Lapierre et al. 2003) are shown for comparison. Samples from the southern Cache Creek plot along the source enrichment trend, and appear to lack any subduction enrichment. Modified after Pearce (1982), and English et al. (2010).

534 **Figure 10:** Rare-earth element (REE) multi-element concentrations relative to N-MORB (Sun
535 and McDonough 1989) for intrusive and extrusive igneous rocks of the Menatatuline Range area.
536 **(A)** Volcanic and volcaniclastic rocks of the Nahlin ophiolite (green triangles) compared to the
537 range of compositions of island-arc tholeiites (IAT) and backarc basin basalts (BABB) in the
538 Nakina transect, and to mafic volcanic rocks from the Kutcho assemblage (white triangles,
539 Childe and Thompson 1997). **(B)** Two E-MORB-type (red triangles) and two OIB-type (blue
540 circles) volcanic rocks from the Menatatuline Range area, compared to the range of compositions
541 of E-MORB and OIB volcanic rocks in the Nakina transect. **(C)** Gabbroic rocks of the Nahlin
542 ophiolite, including dikes ± sills (blue squares) and gabbro pods (red circles). Data from Nakina
543 transect gabbros shown by the grey shaded region. **(D)** Ultramafic and gabbroic cumulates from
544 the Nahlin ophiolite. All data for the Nakina transect (shaded regions) from English et al. (2010).

545 **Figure 11:** Schematic stratigraphic columns for the upper plate, lower plate, and overlap
546 assemblages of the northern Cache Creek terrane based on new and existing geochronological
547 data. Age constraints for lower plate sedimentary rocks after Monger (1975, 1977), Cordey et al.
548 (1991), and Mihalynuk et al. (2003, 2004b). Age constraints for the overlap assemblage
549 sedimentary rocks after Cordey et al. (1991), and Mihalynuk et al. (2003, 2004b), and for the
550 upper plate (ophiolite) assemblage after Gordey et al. (1998), Devine (2002), Mihalynuk et al.
551 (2004b), Zagorevski (2016), and Zagorevski et al. (2016a, 2017).

552 **Figure 12: (A)** Volcanic rock compositions of the Nahlin ophiolite (grey triangles; this study)
553 and correlative Nakina transect BABB and IAT compositions (light and dark grey shaded areas;
554 English et al. 2010) compared to partial melting models. Dot-dashed black line indicates the
555 bulk-peridotite starting composition, and coloured dashed lines reflect segregated melt
556 compositions after 1 - 20% non-modal fractional partial melting of a DMM source in the spinel

stability field. All results normalized to chondrite. **(B)** Bulk-rock REE concentrations for peridotite samples from nearby Peridotite Peak, "Moho Saddle", and Peridotite Peak East (grey circles; Babechuk et al 2010) compared to modeled residue compositions after depletion by 1 – 20% non-modal fractional partial melting of a DMM source in the spinel stability field. All model parameters for (A) and (B) follow those of Warren (2016). Starting bulk-rock composition for DMM is after Workman and Hart (2005), with partition coefficients calculated for a mantle of DMM composition at a potential temperature of 1300 °C (Sun and Liang 2014, Warren 2016). Melting follows the reaction of Wasylenki et al. (2003) for DMM1 composition at 1.0 GPa : 0.56 Opx + 0.72 Cpx + 0.04 Sp = 0.34 Ol + 1.0 Melt.

Figure 13: Potential configurations of the lower plate OIB-carbonate assemblage and the Nahlin ophiolite during the formation of the Nahlin ophiolite as a result of subduction initiation (A, B and C; modified after Maffione et al. 2015), or during spreading in a backarc setting (D) and in a southern Havre Trough-like setting (E). (A) Progressive development of a new subduction zone parallel to a paleo-spreading centre or other pre-existing plane of weakness in the oceanic crust. In response to far-field ridge-perpendicular compression, deformation is localized along a pre-existing detachment fault and an underthrust develops. (B) The underthrust propagates laterally, nucleating a new subduction zone. Fluids are released from the subducting plate. (C) Extension on the overriding plate triggers renewed magmatism along the paleo-spreading centre, thereby forming new SSZ-type crust, preserved in what may later become the forearc region of a mature arc, and thus propensity to be preserved as a SSZ-type ophiolite. (D) Plate configuration for development of the Nahlin ophiolite along a backarc spreading centre. Combination of decompression (dry) and flux melting reconciles the back arc chemistry of the volcanic rocks of the Nahlin ophiolite. (E) Formation of the Nahlin ophiolite in a southern Havre Trough-like

setting, where cross-arc chains of volcanic centres are separated by zone of tectonically accommodated extension erupting back arc basalt along basinal rifts (Wysoczanski et al. 2010). Along-strike variations in volcanic chemistry, from volcanic arc basalts (e.g., Kutcho arc assemblage) to back arc basalt (e.g., arc tholeiites of the Nahlin ophiolite), may explain the lack of preserved arc in the immediate vicinity of the Nahlin ophiolite.

Table 1: Summary of geochronological data constraining the timing of magmatism related to Permo-Triassic arc activity, including evolution of the Nahlin ophiolite, in the northern Cache Creek composite terrane.

Table 2: Lithogeochemical data from plutonic and volcanic rocks of the Menatatuline Range area (n.d. indicates no data).

References

Aitken, J.D. 1959. Atlin map-area, British Columbia (104 N). Geological Survey of Canada Memoir, **307**: 1–89.

Anonymous. 1972. Penrose conference on ophiolites. *In* Geotimes. pp. 22–24.

Ash, C.H. 1994. Origin and tectonic setting of ophiolitic ultramafic rocks in the Atlin area, British Columbia (NTS 104N). *In* Bulletin 94. British Columbia Geological Survey.

Ash, C.H., and Arksey, R.L. 1990. The Atlin ultramafic allochthon: ophiolitic basement within the Cache Creek terrane; tectonic and metallogenic significance. Geological Fieldwork 1989,: 365–374.

Babechuk, M.G., Kamber, B.S., Greig, A., Canil, D., and Kodolányi, J. 2010. The behaviour of tungsten during mantle melting revisited with implications for planetary differentiation time scales. Geochimica et Cosmochimica Acta, **74**: 1448–1470. doi:10.1016/j.gca.2009.11.018.

Barrett, T.J., and MacLean, W.H. 1999. Volcanic sequences, lithogeochemistry, and hydrothermal alteration in some bimodal volcanic-associated massive sulfide systems. *In* Reviews in Economic Geology. pp. 101–131.

Barrett, T.J., Thompson, J.F.H., and Sherlock, R.L. 1996. Stratigraphic, lithogeochemical and tectonic setting of the Kutcho Creek massive sulphide deposit, northern British Columbia. Exploration and Mining Geology, **5**: 309–338.

Bédard, J.H. 1994. A procedure for calculating the equilibrium distribution of trace elements among the minerals of cumulate rocks, and the concentration of trace elements in the coexisting liquids. Chemical Geology, **118**: 143–153. doi:10.1016/0009-2541(94)90173-2.

Bickerton, L., Colpron, M., and Gibson, D. 2012. Cache Creek terrane, Stikinia, and overlap assemblages of eastern Whitehorse (NTS 105D) and western Teslin (NTS 105C) map areas.

Yukon Geological Research,: 1–17.

Bizimis, M., Salters, V.J.M., and Bonatti, E. 2000. Trace and REE content of clinopyroxenes from supra-subduction zone peridotites. Implications for melting and enrichment processes in island arcs. Chemical Geology, **165**: 67–85. doi:10.1016/S0009-2541(99)00164-3.

Bloodgood, M.A., and Bellefontaine, K.A. 1990. The geology of the Atlin area (Dixie Lake and Teresa Island) (104N/6 and parts of 104N/5 and 12). Geological Fieldwork 1989,: 205–215.

Canil, D., Johnston, S.T., and Mihalynuk, M.G. 2006. Mantle redox in Cordilleran ophiolites as a record of oxygen fugacity during partial melting and the lifetime of mantle lithosphere. Earth and Planetary Science Letters, **248**: 91–102. doi:10.1016/j.epsl.2006.04.038.

Childe, F., and Schiarizza, P. 1997. U-Pb geochronology, geochemistry and Nd isotopic systematics of the Sitlika assemblage, central British Columbia. Geological Fieldwork 1996,: 69–78.

Childe, F., and Thompson, J. 1997. Geological setting, U-Pb geochronology, and radiogenic isotopic characteristics of the Permo-Triassic Kutcho Assemblage, north-central British Columbia. Canadian Journal of Earth Sciences, **34**: 1310–1324. Available from http://www.nrcresearchpress.com/doi/abs/10.1139/e17-104.

Cloos, M. 1993. Lithospheric buoyancy and collisional orogenesis: Subduction of oceanic plateaus, continental margins, island arcs, spreading ridges, and seamounts. Geological Association of America Bulletin, **105**: 715–737.

Cordey, F., Gordey, S.P., and Orchard, M.J. 1991. New biostratigraphic data for the northern Cache Creek terrane, Teslin map area, southern Yukon. *In* Current Research, Part E. Geological Survey of Canada. pp. 67–76. doi:10.1126/science.ns-6.149S.521-a.

Devine, F.A.M. 2002. U–Pb geochronology, geochemistry, and tectonic implications of oceanic

637 rocks in the northern Cache Creek Terrane, Nakina area, northwestern British Columbia.
638 University of British Columbia, Vancouver, BC, Canada.
639 Dilek, Y., and Furnes, H. 2009. Structure and geochemistry of Tethyan ophiolites and their
640 petrogenesis in subduction rollback systems. Lithos, **113**: 1–20. Elsevier B.V.
641 doi:10.1016/j.lithos.2009.04.022.
642 Dilek, Y., Furnes, H., and Shallo, M. 2008. Geochemistry of the Jurassic Mirdita Ophiolite
643 (Albania) and the MORB to SSZ evolution of a marginal basin oceanic crust. Lithos, **100**:
644 174–209. doi:10.1016/j.lithos.2007.06.026.
645 English, J.M., and Johnston, S.T. 2005. Collisional orogenesis in the northern Canadian
646 Cordillera: Implications for Cordilleran crustal structure, ophiolite emplacement,
647 continental growth, and the terrane hypothesis. Earth and Planetary Science Letters, **232**:
648 333–344. doi:10.1016/j.epsl.2005.01.025.
649 English, J.M., Mihalynuk, M.G., and Johnston, S.T. 2010. Geochemistry of the northern Cache
650 Creek terrane and implications for accretionary processes in the Canadian Cordillera.
651 Canadian Journal of Earth Sciences, **47**: 13–34. doi:10.1139/E09-066.
652 English, J.M., Mihalynuk, M.G., Johnston, S.T., and Devine, F.A.M. 2002. Atlin TGI Part III :
653 Geology and petrochemistry of mafic rocks within the northern Cache Creek terrane and
654 tectonic implications. Geological Fieldwork 2001,: 19–30.
655 Gabrielse, H. 1991. Late Paleozoic and Mesozoic terrane interactions in north-central British-
656 Columbia. Canadian Journal of Earth Sciences, **28**: 947–957. doi:10.1139/e91-086.
657 Gabrielse, H. 1998. Geology of Cry Lake and Dease Lake map areas, north-central British
658 Columbia. *In* Geological Survey of Canada Bulletin. Geological Survey of Canada Bulletin
659 504. doi:10.1073/pnas.0703993104.

660 Gabrielse, H., Monger, J.W.H., Wheeler, J.O., and Yorath, C.J. 1991. Tectonic Framework, Part
661 A: Morphogeological belts, tectonic assemblages and terranes. *In* Geology of the
662 Cordilleran Orogen in Canada. *Edited by* H. Gabrielse and C.J. Yorath. Geological Survey
663 of Canada. pp. 15–28.
664 Gale, A., Dalton, C.A., Langmuir, C.H., Su, Y., and Schilling, J.G. 2013. The mean composition
665 of ocean ridge basalts. Geochemistry, Geophysics, Geosystems, **14**: 489–518.
666 doi:10.1029/2012GC004334.
667 Gordey, S.P., McNicoll, V.J., and Mortensen, J.K. 1998. New U-Pb ages from the Teslin area,
668 southern Yukon, and their bearing on terrane evolution in the northern Cordillera. *In*
669 Current Research 1998-F Radiogenic age and isotopic studies: Report 11. Geological
670 Survey of Canada. pp. 129–148.
671 Ishizuka, O., Tani, K., Reagan, M.K., Kanayama, K., Umino, S., Harigane, Y., Sakamoto, I.,
672 Miyajima, Y., Yuasa, M., and Dunkley, D.J. 2011. The timescales of subduction initiation
673 and subsequent evolution of an oceanic island arc. Earth and Planetary Science Letters, **306**:
674 229–240. Elsevier B.V. doi:10.1016/j.epsl.2011.04.006.
675 Jenner, G.A. 1996. Trace element geochemistry of igneous rocks: geochemical nomenclature and
676 analytical geochemistry. *In* Trace element geochemistry of volcanic rocks: Applications for
677 massive sulphide exploration. *Edited by* D.A. Wyman. Geological Association of Canada,
678 Short Course Notes. pp. 51–77. Available from
679 http://sparky2.esd.mun.ca/~spiercey/Piercey_Research_Site/ES4502_6510_files/Jenner_19
680 96.pdf.
681 Johnston, S.T., and Borel, G.D. 2007. The odyssey of the Cache Creek terrane, Canadian
682 Cordillera: Implications for accretionary orogens, tectonic setting of Panthalassa, the Pacific

683 superwell, and break-up of Pangea. Earth and Planetary Science Letters, **253**: 415–428.
684 doi:10.1016/j.epsl.2006.11.002.
685 Kelemen, P.B., and Dick, H.J.B. 1995. Focused melt flow and localized deformation in the upper
686 mantle: Juxtaposition of replacive dunite and ductile shear zones in the Josephine peridotite,
687 SW Oregon. Journal of Geophysical Research, **100**: 423–438. doi:10.1029/94JB02063.
688 Kimura, G., and Ludden, J. 1995. Peeling oceanic crust in subduction zones. Geology, **23**: 217–
689 220. doi:10.1130/0091-7613(1995)023<0217.
690 Kinzler, R.J., and Grove, T.L. 1992. Primary magmas of mid-ocean ridge basalts 2. Applications.
691 Journal of Geophysical Research, **97**: 6907–6926. doi:10.1029/91JB02841.
692 Lagabrielle, Y., Vitale Brovarone, A., and Ildefonse, B. 2015. Fossil oceanic core complexes
693 recognized in the blueschist metaophiolites of Western Alps and Corsica. Earth-Science
694 Reviews, **141**: 1–26. Elsevier B.V. doi:10.1016/j.earscirev.2014.11.004.
695 Langmuir, C.H. 1989. Geochemical consequences of in situ crystallization.
696 doi:10.1038/340199a0.
697 Lapierre, H., Bosch, D., Tardy, M., and Struik, L.C. 2003. Late Paleozoic and Triassic plume-
698 derived magmas in the Canadian Cordillera played a key role in continental crust growth.
699 Chemical Geology, **201**: 55–89. doi:10.1016/S0009-2541(03)00224-9.
700 MacLean, W.H. 1990. Mass change calculations in altered rock series. Mineralium Deposita, **25**:
701 44–49. doi:10.1007/BF03326382.
702 Maffione, M., Morris, A., and Anderson, M.W. 2013. Recognizing detachment-mode seafloor
703 spreading in the deep geological past. Scientific reports, **3**: 2336. doi:10.1038/srep02336.
704 Maffione, M., Thieulot, C., Van Hinsbergen, D.J.J., Morris, A., Plumper, O., and Spakman, W.
705 2015. Dynamics of intraoceanic subduction initiation: 1. Oceanic detachment fault inversion

and the formation of supra-subduction zone ophiolites. Geochemistry Geophysics Geosystems, **16**: 1753–1770. doi:10.1002/2015GC005745.Dynamics.

Le Maitre, R.W. 1989. A classification of igneous rocks and glossary of terms. Blackwell Books, Oxford, UK.

McGoldrick, S., Zagorevski, A., Canil, D., Corriveau, A.-S., Bichlmaier, S., and Carroll, S. 2016. Geology of the Cache Creek terrane in the Peridotite Peak – Menatatuline Range Area, northwestern British Columbia (Parts of NTS 104K/15 , /16). Geoscience BC Summary of Activities 2015,: 149–162.

Merran, Y. 2002. Mise en place et environnement de depot d'une plate-forme carbonatée intraoceanique: example du complexe d'Atlin, Canada. Université Claude Bernard, France.

Mihalynuk, M.G. 1999. Geology and mineral resources of the Tagish Lake area (NTS 104M/8,9,10E,15 and 104N/12W) northwestern British Columbia. *In* Bulletin 105. British Columbia Geological Survey.

Mihalynuk, M.G., Bellefontaine, K.A., Brown, D.A., Logan, J.M., Nelson, J.L., Legun, A.S., and Diakow, L.J. 1996. Geological compilation, northwest British Columbia (NTS 94E, L, M; 104F, G, H, I, J, K, L, M, N, O, P; 114J, O, P). BC Ministry of Energy and Mines.

Mihalynuk, M.G., and Cordey, F. 1997. Potential for Kutcho Creek volcanogenic massive sulphide mineralization in the northern Cache Creek terrane: a progress report. Geological Fieldwork 1996,: 157–170.

Mihalynuk, M.G., Erdmer, P., Ghent, E.D., Archibald, D.A., Friedman, R.M., Cordey, F., Johannson, G.G., and Beanish, J. 1998. Age constraints for emplacement of the northern cache creek terrane and implications of blueschist metamorphism. Geological Fieldwork 1997,: 127–141.

729 Mihalynuk, M.G., Erdmer, P., Ghent, E.D., Cordey, F., Archibald, D.A., Friedman, R.M., and
730 Johannson, G.G. 2004a. Coherent French Range blueschist: Subduction to exhumation in
731 less than 2.5 m.y.? Geological Society of America Bulletin, **116**: 910–922.
732 doi:10.1130/B25393.1.
733 Mihalynuk, M.G., Fiererra, L., Robertson, S., Devine, F.A.M., and Cordey, F. 2004b. Geology
734 and new mineralization in the Joss'alun belt, Atlin area. Geological Fieldwork 2003,: 61–
735 82.
736 Mihalynuk, M.G., Johnston, S.T., English, J.M., Cordey, F., Villeneuve, M.E., Rui, L., and
737 Orchard, M.J. 2003. Atlin TGI , Part II : Regional geology and mineralization of the Nakina
738 area (NTS 104N / 2W and 3). Geological Fieldwork 2002,: 9–38.
739 Mihalynuk, M.G., Johnston, S.T., Lowe, C., Cordey, F., English, J.M., Devine, F.A.M., Larson,
740 K., and Merran, Y. 2002. Atlin TGI Part II : Preliminary results from the Atlin Targeted
741 Geoscience Initiative, Nakina area, northwest British Columbia. Geological Fieldwork
742 2001,: 5–18.
743 Mihalynuk, M.G., Nelson, J.A., and Diakow, L.J. 1994. Cache Creek terrane entrapment:
744 oroclinal paradox within the Canadian Cordillera. Tectonics, **13**: 575–595.
745 doi:10.1029/93TC03492.
746 Mihalynuk, M.G., Smith, M.T., Gabites, J.E., Runkle, D., and Lefebure, D. 1992. Age of
747 emplacement and basement character of the Cache Creek terrane as constrained by new
748 isotopic and geochemical data. Canadian Journal of Earth Sciences, **29**: 2463–2477.
749 doi:10.1139/e92-193.
750 Monger, J.W.H. 1975. Upper Paleozoic rocks of the Atlin terrane, northwestern British
751 Columbia and south-central Yukon. Geological Survey of Canada Paper 74-47.

752 Monger, J.W.H. 1977. Upper Paleozoic rocks of northwestern British Columbia. *In* Report of
753 Activities, Part A. Geological Survey of Canada. pp. 255–262. doi:10.1038/074245b0.
754 Monger, J.W.H., and Ross, C.A. 1971. Distribution of Fusulinaceans in the western Canadian
755 Cordillera. Canadian Journal of Earth Sciences, **8**: 259–278. doi:10.1139/e71-026.
756 Natural Resources Canada. 1990a. Teditua Creek NTS 104K/16, 1:50 000 scale raster image.
757 Natural Resources Canada.
758 Natural Resources Canada. 1990b. Yeth Creek NTS 104K/15, 1:50 000 scale raster image.
759 Natural Resources Canada.
760 Nelson, J.A., and Colpron, M. 2007. Tectonics and metallogeny of the British Columbia, Yukon
761 and Alaskan Cordillera, 1.8 Ga to the present. *In* Mineral Deposits of Canada: A synthesis
762 of major deposit types, district metallogeny, the evolution of geological provinces, and
763 exploration methods. *Edited by* W.D. Goodfellow. Geological Association of Canada,
764 Mineral Deposits Division. pp. 755–791.
765 Nelson, J.A., and Colpron, M. 2011. A digital atlas of terranes for the northern Cordillera.
766 Niu, Y.L., and Batiza, R. 1991. An empirical method for calculating melt compositions produced
767 beneath ridges: Application for axis and off-axis (seamounts) melting. Journal of
768 Geophysical Research, **96**: 21753–21777.
769 Ohara, Y., Fujioka, K., Ishii, T., and Yurimoto, H. 2003. Peridotites and gabbros from the Parece
770 Vela backarc basin: Unique tectonic window in an extinct backarc spreading ridge.
771 Geochemistry, Geophysics, Geosystems, **4**: n/a-n/a. doi:10.1029/2002GC000469.
772 Orchard, M.J., Cordey, F., Rui, L., Bamber, E.W., Mamet, B., Struik, L.C., Sano, H., and Taylor,
773 H.J. 2001. Biostratigraphic and biogeographic constraints on the Carboniferous to Jurassic
774 Cache Creek Terrane in central British Columbia. Canadian Journal of Earth Sciences, **38**:

551–578. doi:10.1139/e00-120.

Pearce, J.A. 1982. Trace element characteristics of lavas from destructive plate boundaries. *In* Orogenic andesites and related rocks. *Edited by* R.S. Thorpe. John Wiley and Sons, Chichester, UK. pp. 525–548.

Pearce, J.A. 1996. A user's guide to basalt discrimination diagrams. *In* Trace element geochemistry of volcanic rocks: Applications for massive sulphide exploration. *Edited by* D.A. Wyman. Geological Association of Canada, Short Course Notes. pp. 79–113.

Pearce, J.A., and Norry, M.J. 1979. Petrogenetic implications of Ti, Zr, Y, and Nb variations in volcanic rocks. Contributions to Mineralogy and Petrology, **69**: 33–47. doi:10.1007/BF00375192.

Pearce, J.A., and Peate, D.W. 1995. Tectonic implications of the composition of volcanic arc magmas. Annual Review of Earth and Planetary Sciences, **23**: 251–285.

Pomonis, P., Tsikouras, B., and Hatzipanagiotou, K. 2006. Petrogenetic evolution of the Koziakas ophiolite complex (W. Thessaly, Greece). Mineralogy and Petrology, **89**: 77–111. doi:10.1007/s00710-006-0138-4.

Reagan, M.K., Ishizuka, O., Stern, R.J., Kelley, K.A., Ohara, Y., Blichert-Toft, J., Bloomer, S.H., Cash, J., Fryer, P., Hanan, B.B., Hickey-Vargas, R., Ishii, T., Kimura, J.I., Peate, D.W., Rowe, M.C., and Woods, M. 2010. Fore-arc basalts and subduction initiation in the Izu-Bonin-Mariana system. Geochemistry, Geophysics, Geosystems, **11**: 1–17. doi:10.1029/2009GC002871.

Reagan, M.K., McClelland, W.C., Girard, G., Goff, K.R., Peate, D.W., Ohara, Y., and Stern, R.J. 2013. The geology of the southern Mariana fore-arc crust: Implications for the scale of Eocene volcanism in the western Pacific. Earth and Planetary Science Letters, **380**: 41–51.

Elsevier B.V. doi:10.1016/j.epsl.2013.08.013.

Ross, P.-S., and Bédard, J.H. 2009. Magmatic affinity of modern and ancient subalkaline volcanic rocks determined from trace-element discriminant diagrams. Canadian Journal of Earth Sciences, **46**: 823–839. doi:10.1139/E09-054.

Saccani, E., and Photiades, A. 2004. Mid-ocean ridge and supra-subduction affinities in the Pindos ophiolites (Greece): Implications for magma genesis in a forearc setting. Lithos, **73**: 229–253. doi:10.1016/j.lithos.2003.12.002.

Saunders, A.D., Norry, M., and Tarney, J. 1988. Origin of MORB and chemically-depleted mantle reservoirs: Trace element constraints. Journal of Petrology,: 415–445.

Schiarizza, P. 2012. Geology of the Kutcho assemblage between the Kehlechoa and Tucho Rivers, northern British Columbia (NTS 104I / 01 , 02). Geological Fieldwork 2011,: 75–98.

Smith, I.E.M., and Price, R.C. 2006. The Tonga-Kermadec arc and Havre-Lau back-arc system: Their role in the development of tectonic and magmatic models for the western Pacific. Journal of Volcanology and Geothermal Research, **156**: 315–331. doi:10.1016/j.jvolgeores.2006.03.006.

Souther, J.G. 1971. Geology and mineral deposits of Tulsequah map area, British Columbia (104K). Geological Survey of Canada Memoir, **362**: 1–84. doi:10.1017/CBO9781107415324.004.

Stern, R.J., Reagan, M.K., Ishizuka, O., Ohara, Y., and Whattam, S.A. 2012. To understand subduction initiation, study forearc crust: To understand forearc crust, study ophiolites. Lithosphere,: 469–483. doi:10.1130/L183.1.

Struik, L.C., Schiarizza, P., Orchard, M.J., Cordey, F., Sano, H., MacIntyre, D.G., Lapierre, H.,

and Tardy, M. 2001. Imbricate architecture of the upper Paleozoic to Jurassic oceanic Cache Creek Terrane, central British Columbia. Canadian Journal of Earth Sciences, **38**: 495–514. doi:10.1139/cjes-38-4-495.

Sun, C., and Liang, Y. 2014. An assessment of subsolidus re-equilibration on REE distribution among mantle minerals olivine, orthopyroxene, clinopyroxene, and garnet in peridotites. Chemical Geology, **372**: 80–91. Elsevier B.V. doi:10.1016/j.chemgeo.2014.02.014.

Sun, S., and McDonough, W.F. 1989. Chemical and isotopic systematics of oceanic basalts: implications for mantle composition and processes. *In* Magmatism in the ocean basins. *Edited by* A.D. Saunders and M.J. Norry. Geological Society of London. pp. 313–345.

Tamura, Y., Tatsumi, Y., Zhao, D., Kido, Y., and Shukuno, H. 2002. Hot fingers in the mantle wedge: New insights into magma genesis in subduction zones. Earth and Planetary Science Letters, **197**: 105–116. doi:10.1016/S0012-821X(02)00465-X.

Tardy, M., Lapierre, H., Struik, L.C., Bosch, D., and Brunet, P. 2001. The influence of mantle plume in the genesis of the Cache Creek oceanic igneous rocks: implications for the geodynamic evolution of the inner accreted terranes of the Canadian Cordillera. Canadian Journal of Earth Sciences, **38**: 515–534.

Tempelman-Kluit, D.J. 1979. Transported cataclasite, ophiolite and granodiorite in Yukon: Evidence of arc-continent collision. Geological Survey of Canada Paper 79-14.

Terry, J. 1977. Geology of the Nahlin ultramafic body, Atlin and Tulsequah map-areas, northwestern British Columbia. *In* Report of Activities, Part A. Geological Survey of Canada. pp. 263–269.

Todd, E., Gill, J.B., Wysoczanski, R.J., Hergt, J., Wright, I.C., Leybourne, M.I., and Mortimer, N. 2011. Hf isotopic evidence for small-scale heterogeneity in the mode of mantle wedge

844 enrichment: Southern Havre Trough and South Fiji Basin back arcs. Geochemistry,
845 Geophysics, Geosystems, **12**. doi:10.1029/2011GC003683.
846 Uysal, I., Ersoy, E.Y., Dilek, Y., Kapsiotis, A., and Sarıfakıoğlu, E. 2016. Multiple episodes of
847 partial melting, depletion, metasomatism and enrichment processes recorded in the
848 heterogeneous upper mantle sequence of the Neotethyan Eldivan ophiolite, Turkey. Lithos,
849 **246**–**247**: 228–245. doi:10.1016/j.lithos.2016.01.004.
850 Warren, J.M. 2016. Global variations in abyssal peridotite compositions. Lithos, **248**–**251**: 193–
851 219. The Author. doi:10.1016/j.lithos.2015.12.023.
852 Warren, J.M., and Shimizu, N. 2010. Cryptic variations in abyssal peridotite compositions:
853 Evidence for shallow-level melt infiltration in the oceanic lithosphere. Journal of Petrology,
854 **51**: 395–423. doi:10.1093/petrology/egp096.
855 Wasylenki, L.E., Baker, M.B., Kent, A.J.R., and Stolper, E.M. 2003. Near-solidus melting of the
856 shallow upper mantle: Partial melting experiments on depleted peridotite. Journal of
857 Petrology, **44**: 1163–1191. doi:10.1093/petrology/44.7.1163.
858 Whattam, S.A., and Stern, R.J. 2011. The "subduction initiation rule": A key for linking
859 ophiolites, intra-oceanic forearcs, and subduction initiation. Contributions to Mineralogy
860 and Petrology, **162**: 1031–1045. doi:10.1007/s00410-011-0638-z.
861 Wilson, S.C., Murton, B.J., and Taylor, R.N. 2013. Mantle composition controls the
862 development of an Oceanic Core Complex. Geochemistry, Geophysics, Geosystems, **14**:
863 979–995. doi:10.1002/ggge.20046.
864 Workman, R.K., and Hart, S.R. 2005. Major and trace element composition of the depleted
865 MORB mantle (DMM). Earth and Planetary Science Letters, **231**: 53–72.
866 doi:10.1016/j.epsl.2004.12.005.

867 Wysoczanski, R.J., Todd, E., Wright, I.C., Leybourne, M.I., Hergt, J.M., Adam, C., and Mackay,
868 K. 2010. Backarc rifting, constructional volcanism and nascent disorganised spreading in
869 the southern Havre Trough backarc rifts (SW Pacific). Journal of Volcanology and
870 Geothermal Research, **190**: 39–57. Elsevier B.V. doi:10.1016/j.jvolgeores.2009.04.004.
871 Zagorevski, A. 2016. Geochemical data of the northern Cache Creek and Stikine terranes and
872 their overlap assemblages, British Columbia and Yukon. Geological Survey of Canada
873 Open File, **8039**: 1–11. doi:10.4095/299347.
874 Zagorevski, A., Corriveau, A.-S., McGoldrick, S., Bédard, J.H., Canil, D., Golding, M.L., Joyce,
875 N., and Mihalynuk, M.G. 2015. Geological framework of ancient oceanic crust in
876 northwestern British Columbia and southwestern Yukon GEM 2 Cordillera. Geological
877 Survey of Canada Open File, **7957**: 1–10. doi:10.4095/297273.
878 Zagorevski, A., Lissenberg, C.J., and van Staal, C.R. 2009. Dynamics of accretion of arc and
879 backarc crust to continental margins: Inferences from the Annieopsquotch accretionary
880 tract, Newfoundland Appalachians. Tectonophysics, **479**: 150–164. Elsevier B.V.
881 doi:10.1016/j.tecto.2008.12.002.
882 Zagorevski, A., Mihalynuk, M.G., Joyce, N., and Anderson, R.G. 2017. Late Cretaceous
883 magmatism in the Atlin-Tagish area, northern British Columbia (104M , 104N). Geological
884 Fieldwork 2016,: 133–152.
885 Zagorevski, A., Mihalynuk, M.G., McGoldrick, S., Bédard, J.H., Golding, M.L., Joyce, N.,
886 Lawley, C., Canil, D., Corriveau, A.-S., Bogatu, A., and Tremblay, A. 2016a. Geological
887 framework of ancient oceanic crust in northwestern British Columbia and southwestern
888 Yukon GEM 2 Cordillera. Geological Survey of Canada Open File, **8140**: 1–13.
889 doi:10.4095/297273.

Zagorevski, A., Mihalynuk, M.G., Milidragovic, D., Joyce, N., Kovacs, N., Allan, M., Friedman, R.M., and Kellett, D.A. 2016b. Characterization of volcanic and intrusive rocks across the British Columbia - Yukon border, GEM 2 Cordillera. Geological Survey of Canada Open File, **8141**: 1–13. doi:10.4095/297272.

Zagorevski, A., and van Staal, C.R. 2011. The Record of Ordovician arc-arc and arc-continent collisions in the Canadian Appalachians during the closure of Iapetus. *In* Frontiers in Earth Sciences. *Edited by* D. Brown and P.D. Ryan. Springer-Verlag Berlin Heidelberg. pp. 341–371. doi:10.1007/978-3-540-88558-0.

Table 1: Summary of ophiolitic and arc rocks in the northern Cache Creek terrane

Map	Location	Lithologies	Affinity
A	King Mountain (BC)	ophiolite, mantle, gabbro, dykes	IAT, BON
B	Kutcho	bimodal volcanic rocks	IAT
C	Nakina area (BC)	quartz diorite intruding into mantle	IAT
D	Tseta Creek (BC)	diorite in mafic volcanic and intrusive rocks	IAT
E	Graham Creek (BC)	basalt, diabase, mantle and chert	BAB
F	Jakes Corner (YK)	gabbro stitching mantle and basalt	IAT
G	Teslin (YK)	trondhjemite in ophiolite	IAT

*[1]Zagorevski et al. (2016a), [2]Zagorevski et al.(2016c), [3]Schiarrizza (2011), [4]Childe and Thomp
[7]Mihalynuk et al. (2003), [8]Mihalynuk et al. (1998); [9]Zagorevski et al. (2017) [10]Gordey et al. (

Method	Age (Ma)	Reference*
U-Pb zrn, ttn; Ar-Ar hbl	ca. 250-255	1, 2
U-Pb zrn	ca. 242-251.71	3, 4
U-Pb zrn	255±2.8	5, 6, 2
U-Pb zrn	261.4±0.3	6, 7
Radiolaria	Middle Triassic	8, 9
U-Pb zrn	ca. 245	1, 2
U-Pb zrn	245.4±0.8	1, 2, 8

ɔson (1997), [5]Devine (2002), [6]English et al. (2010),
1998)

Figure 1

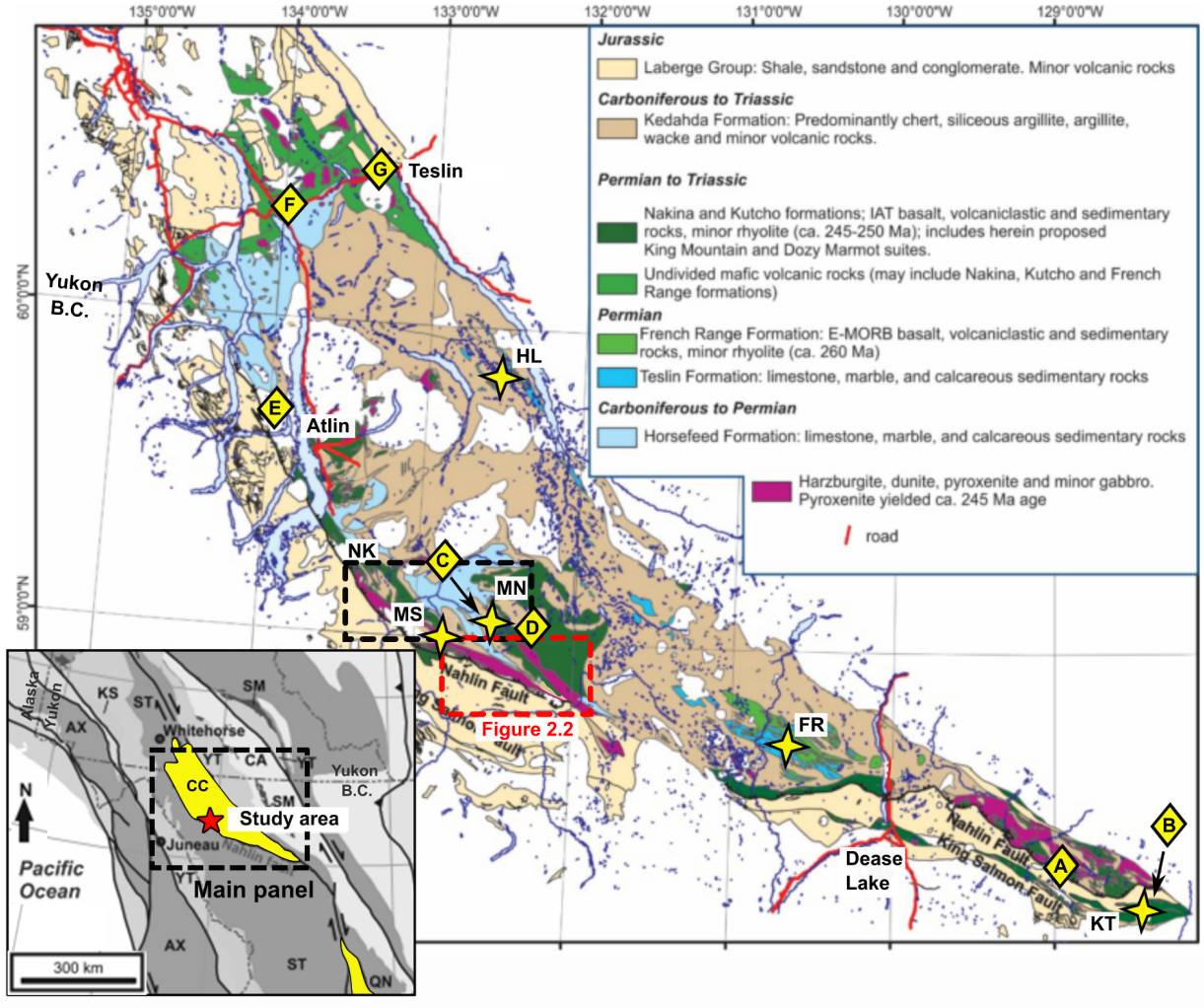
135°0'0"W
134°0'0"W
133°0'0"W
132°0'0"W
131°0'0"W
130°0'0"W
129°0'0"W
60°0'0"N
59°0'0"N
Jurassic
Laberge Group: Shale, sandstone and conglomerate. Minor volcanic rocks
Carboniferous to Triassic
Kedahda Formation: Predominantly chert, siliceous argillite, argillite, wacke and minor volcanic rocks.
Permian to Triassic
Nakina and Kutcho formations; IAT basalt, volcaniclastic and sedimentary rocks, minor rhyolite (ca. 245-250 Ma); includes herein proposed King Mountain and Dozy Marmot suites.
Undivided mafic volcanic rocks (may include Nakina, Kutcho and French Range formations)
Permian
French Range Formation: E-MORB basalt, volcaniclastic and sedimentary rocks, minor rhyolite (ca. 260 Ma)
Teslin Formation: limestone, marble, and calcareous sedimentary rocks
Carboniferous to Permian
Horsefeed Formation: limestone, marble, and calcareous sedimentary rocks
Harzburgite, dunite, pyroxenite and minor gabbro. Pyroxenite yielded ca. 245 Ma age
road
Yukon
B.C.
Teslin
Atlin
HL
NK
MN
MS
Nahlin Fault
Figure 2.2
FR
Dease Lake
King Salmon Fault
KT
A
B
C
D
E
F
G
Alaska
Yukon
KS
ST
SM
AX
Whitehorse
YT
CA
Yukon
B.C.
CC
LSM
Study area
Juneau
Nahlin
Pacific Ocean
Main panel
AX
ST
QN
300 km
N

Figure 2

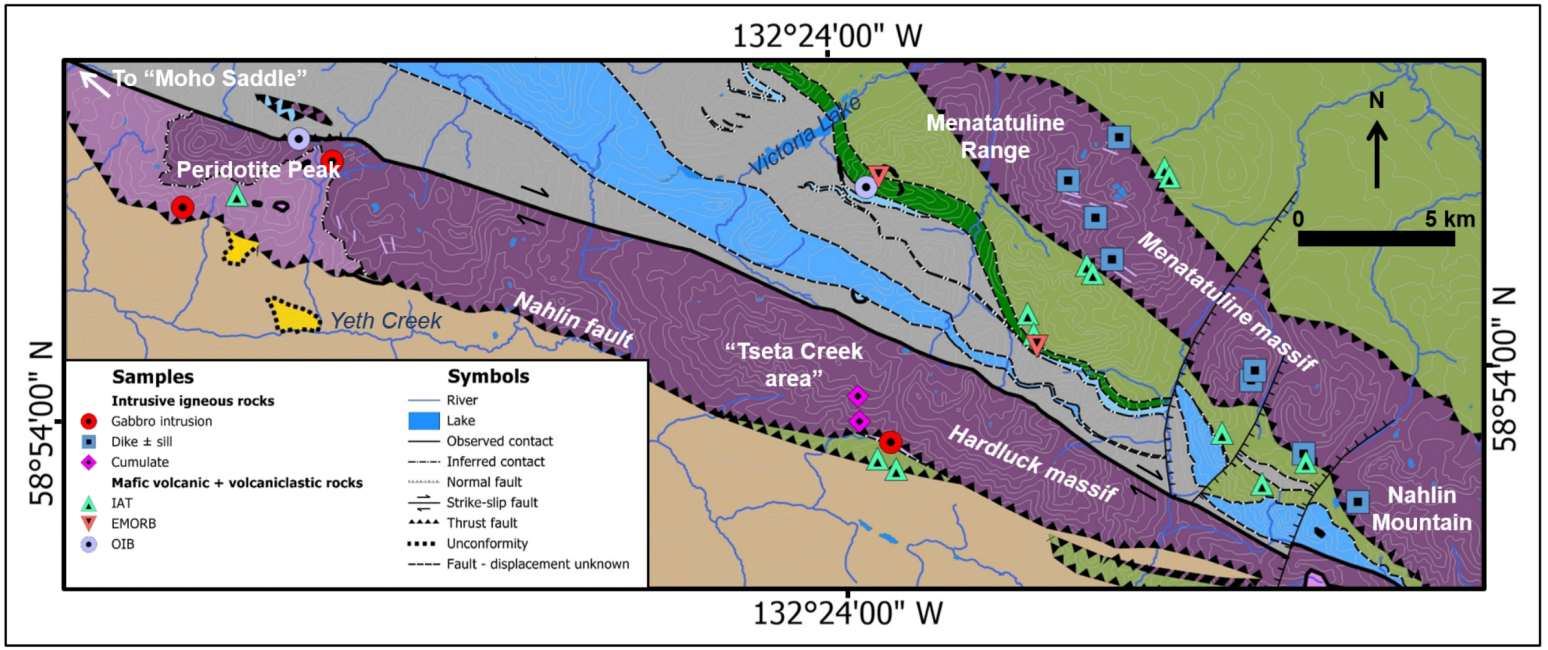
132°24'00" W
To "Moho Saddle"
Peridotite Peak
Yeth Creek
Victoria Lake
Menatatuline Range
Menatatuline massif
Nahlin fault
"Tseta Creek area"
Hardluck massif
Nahlin Mountain
N
0
5 km
58°54'00" N
Samples
Intrusive igneous rocks
Gabbro intrusion
Dike ± sill
Cumulate
Mafic volcanic + volcaniclastic rocks
IAT
EMORB
OIB
Symbols
River
Lake
Observed contact
Inferred contact
Normal fault
Strike-slip fault
Thrust fault
Unconformity
Fault - displacement unknown

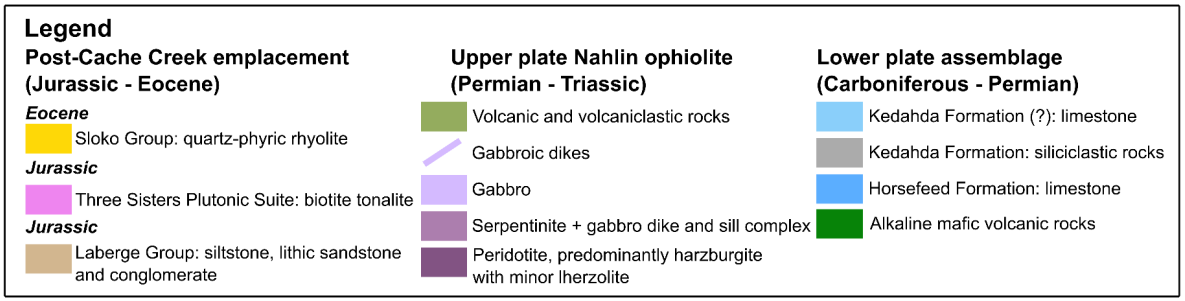
Legend
Post-Cache Creek emplacement (Jurassic - Eocene)
Eocene
Sloko Group: quartz-phyric rhyolite
Jurassic
Three Sisters Plutonic Suite: biotite tonalite
Jurassic
Laberge Group: siltstone, lithic sandstone and conglomerate
Upper plate Nahlin ophiolite (Permian - Triassic)
Volcanic and volcaniclastic rocks
Gabbroic dikes
Gabbro
Serpentinite + gabbro dike and sill complex
Peridotite, predominantly harzburgite with minor lherzolite
Lower plate assemblage (Carboniferous - Permian)
Kedahda Formation (?): limestone
Kedahda Formation: siliciclastic rocks
Horsefeed Formation: limestone
Alkaline mafic volcanic rocks

Figure 3

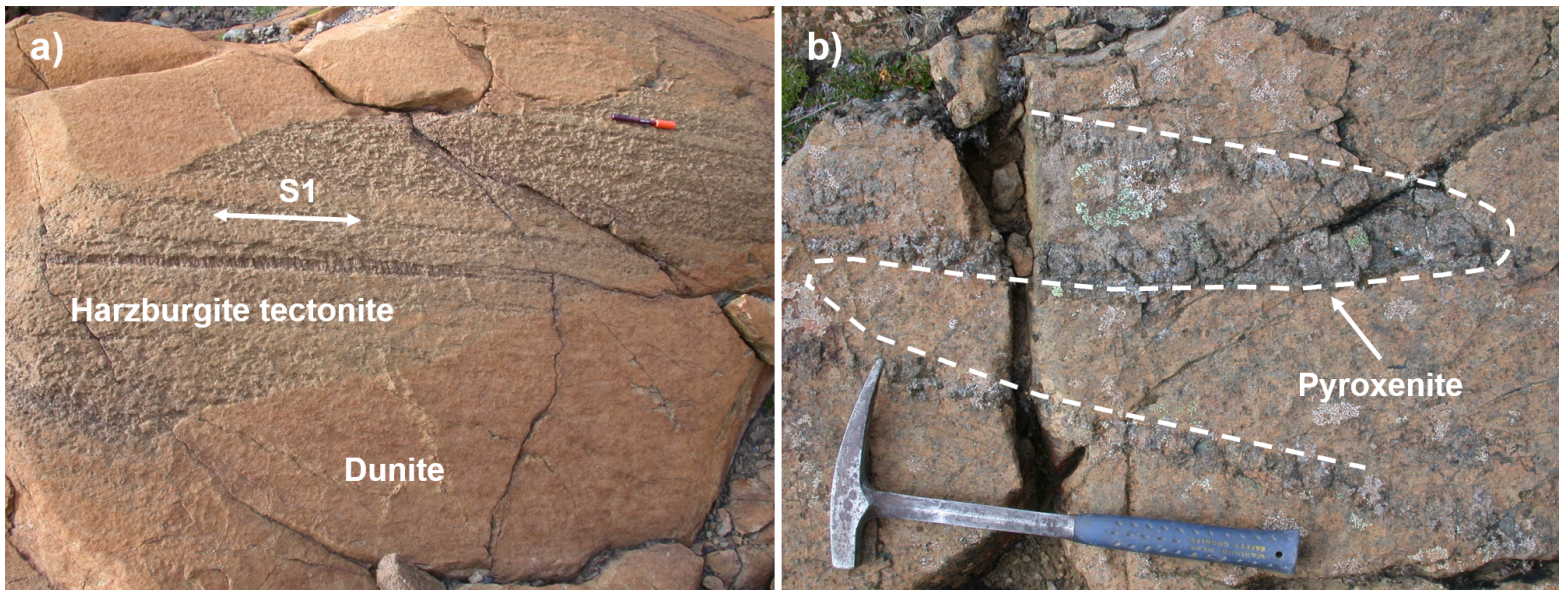

Figure 4

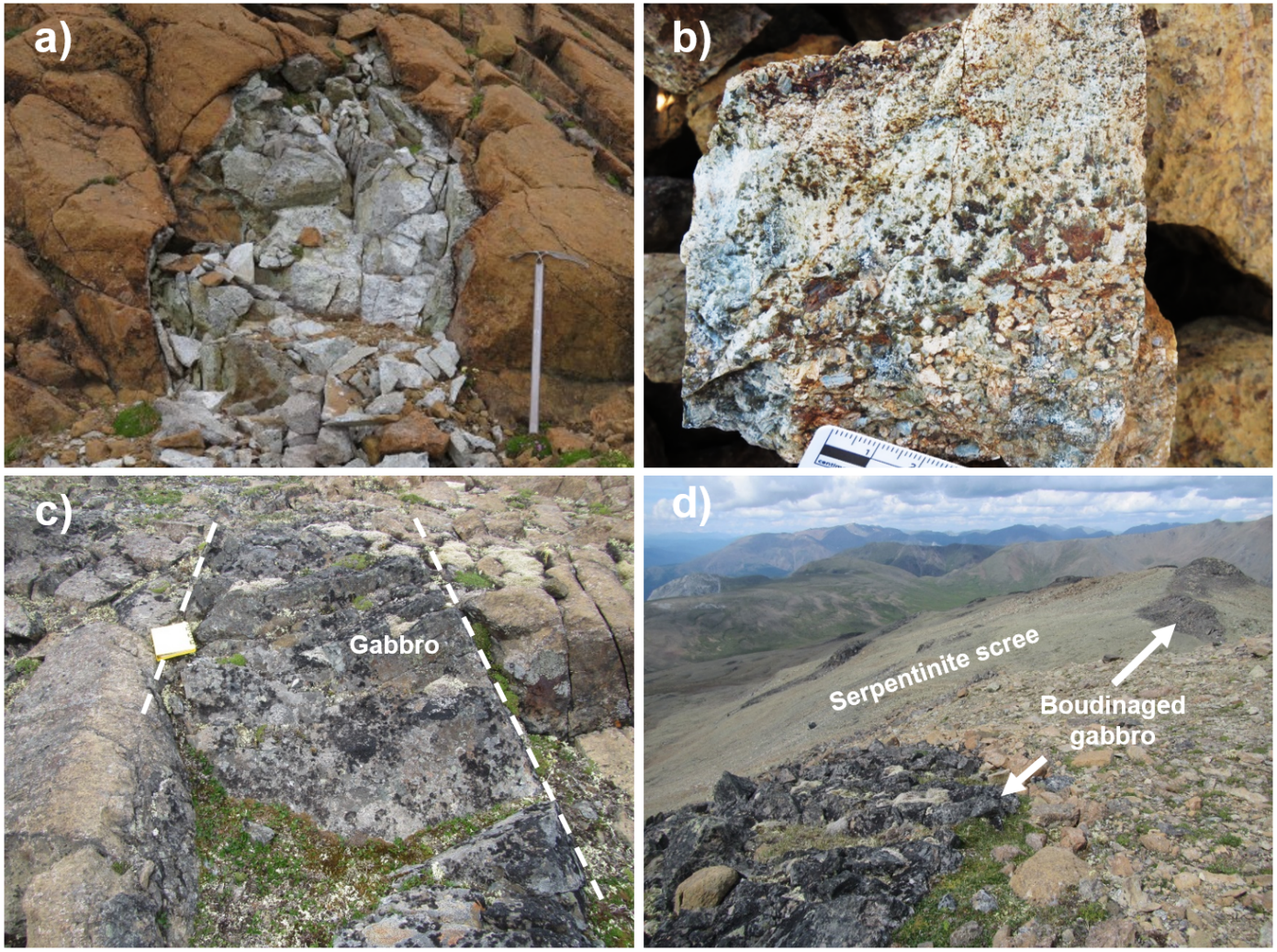

Figure 5

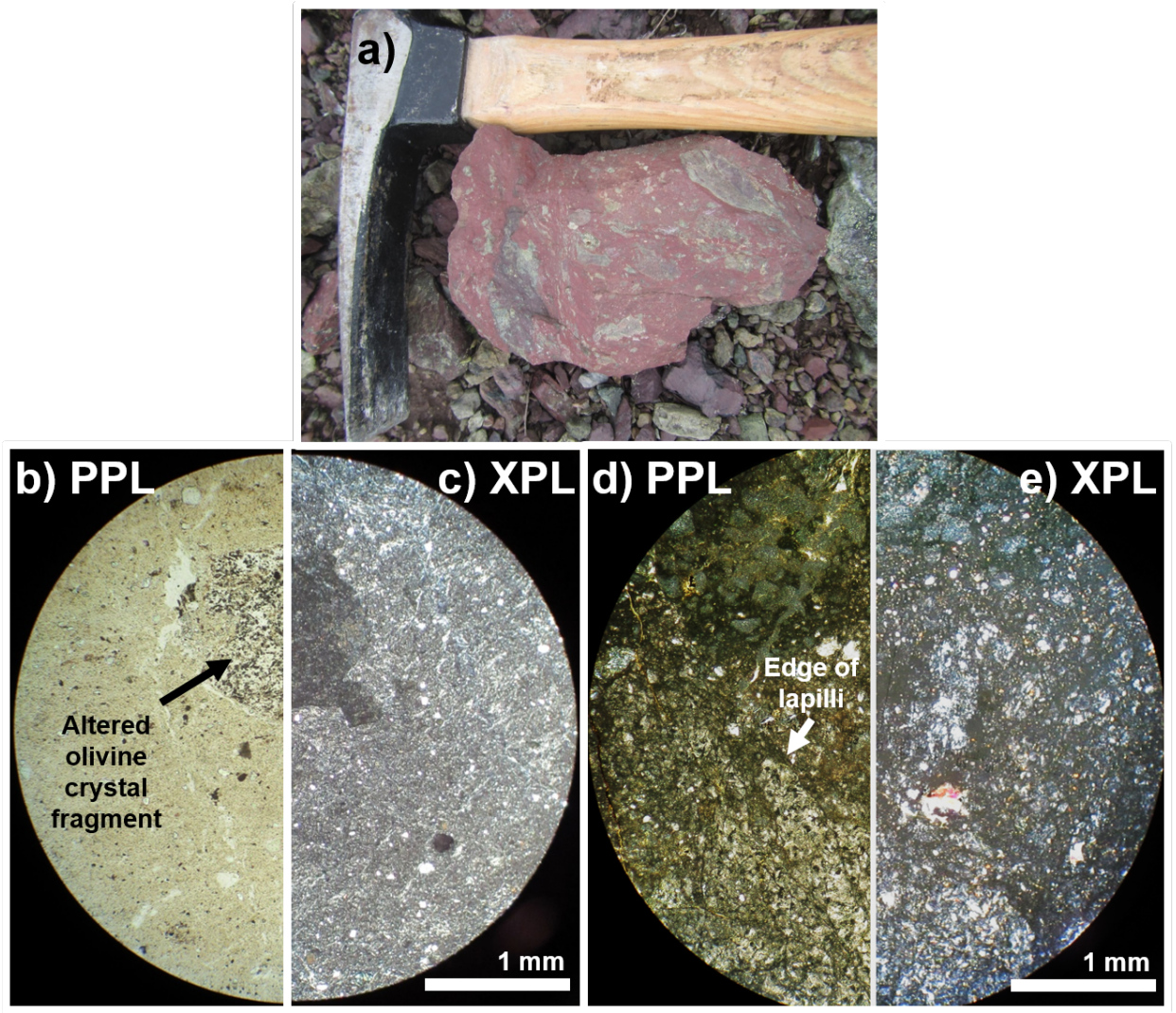
a)
b) PPL
Altered olivine crystal fragment
c) XPL
1 mm
d) PPL
Edge of lapilli
e) XPL
1 mm

Figure 6

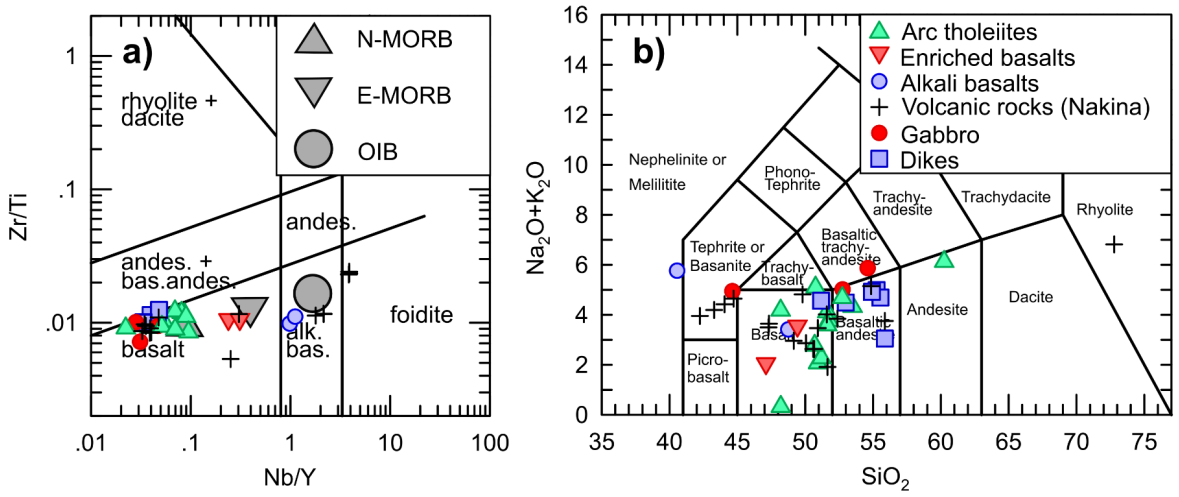
a)
N-MORB
E-MORB
OIB
rhyolite +
dacite
andes.
andes. +
bas.andes.
basalt
alk.
bas.
foidite
Zr/Ti
Nb/Y
1
.1
.01
.01
.1
1
10
100
b)
Arc tholeiites
Enriched basalts
Alkali basalts
Volcanic rocks (Nakina)
Gabbro
Dikes
Nephelinite or
Melilitite
Phono-
Tephrite
Trachy-
andesite
Trachydacite
Rhyolite
Tephrite or
Basanite
Trachy-
basalt
Basaltic
trachy-
andesite
Andesite
Dacite
Basaltic
andesite
Picro-
basalt
Na2O+K2O
SiO2
0
2
4
6
8
10
12
14
16
35
40
45
50
55
60
65
70
75

Figure 7

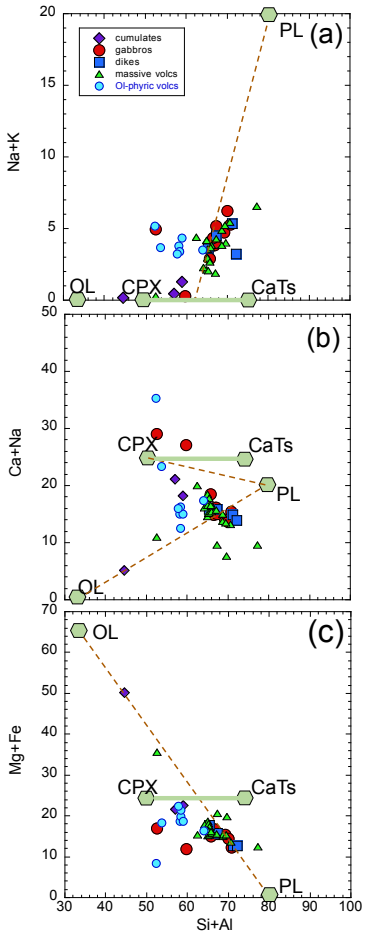
cumulates
gabbros
dikes
massive volcs
Ol-phyric volcs
(a)
PL
OL
CPX
CaTs
Na+K
(b)
CPX
CaTs
PL
OL
Ca+Na
(c)
OL
CPX
CaTs
PL
Mg+Fe
Si+Al

Figure 8

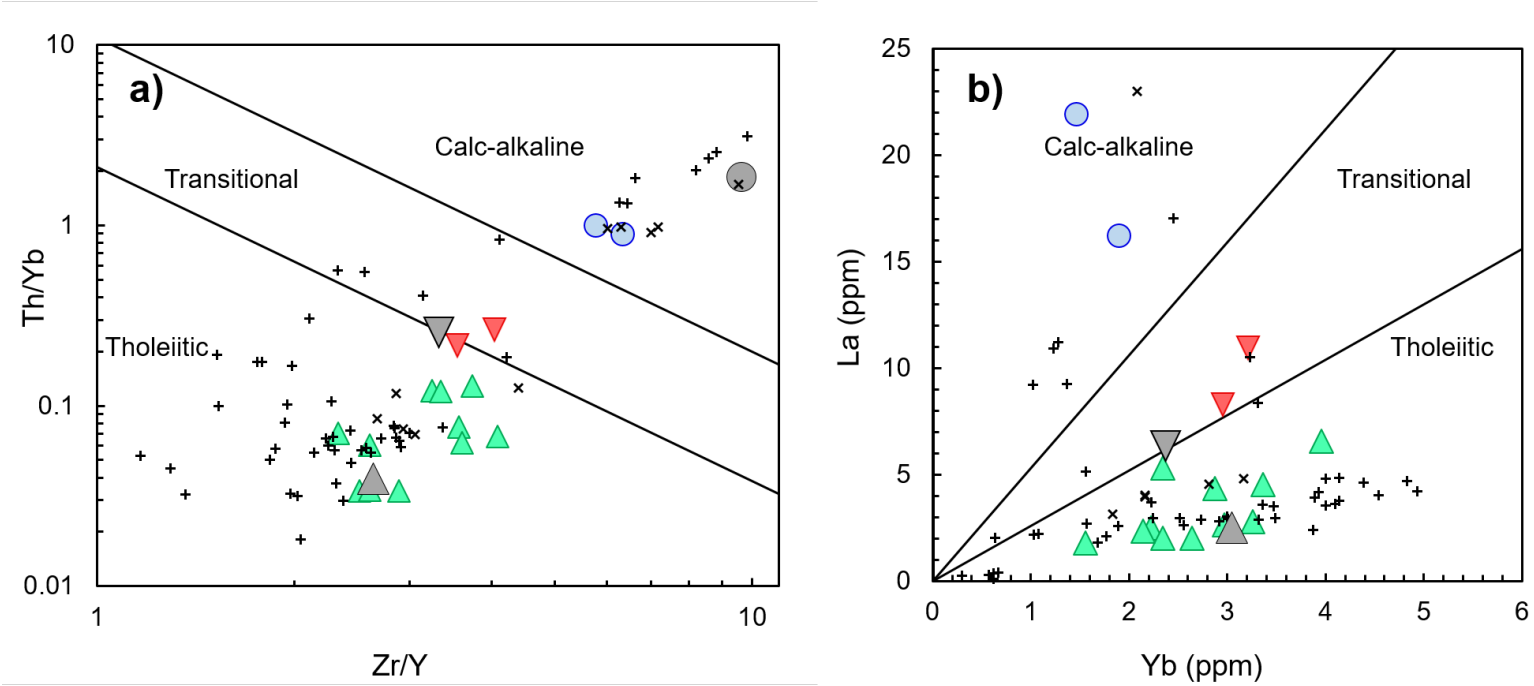
a)
Calc-alkaline
Transitional
Tholeiitic
Th/Yb
Zr/Y
10
1
0.1
0.01
1
10
b)
Calc-alkaline
Transitional
Tholeiitic
La (ppm)
Yb (ppm)
25
20
15
10
5
0
0
1
2
3
4
5
6

Figure 9

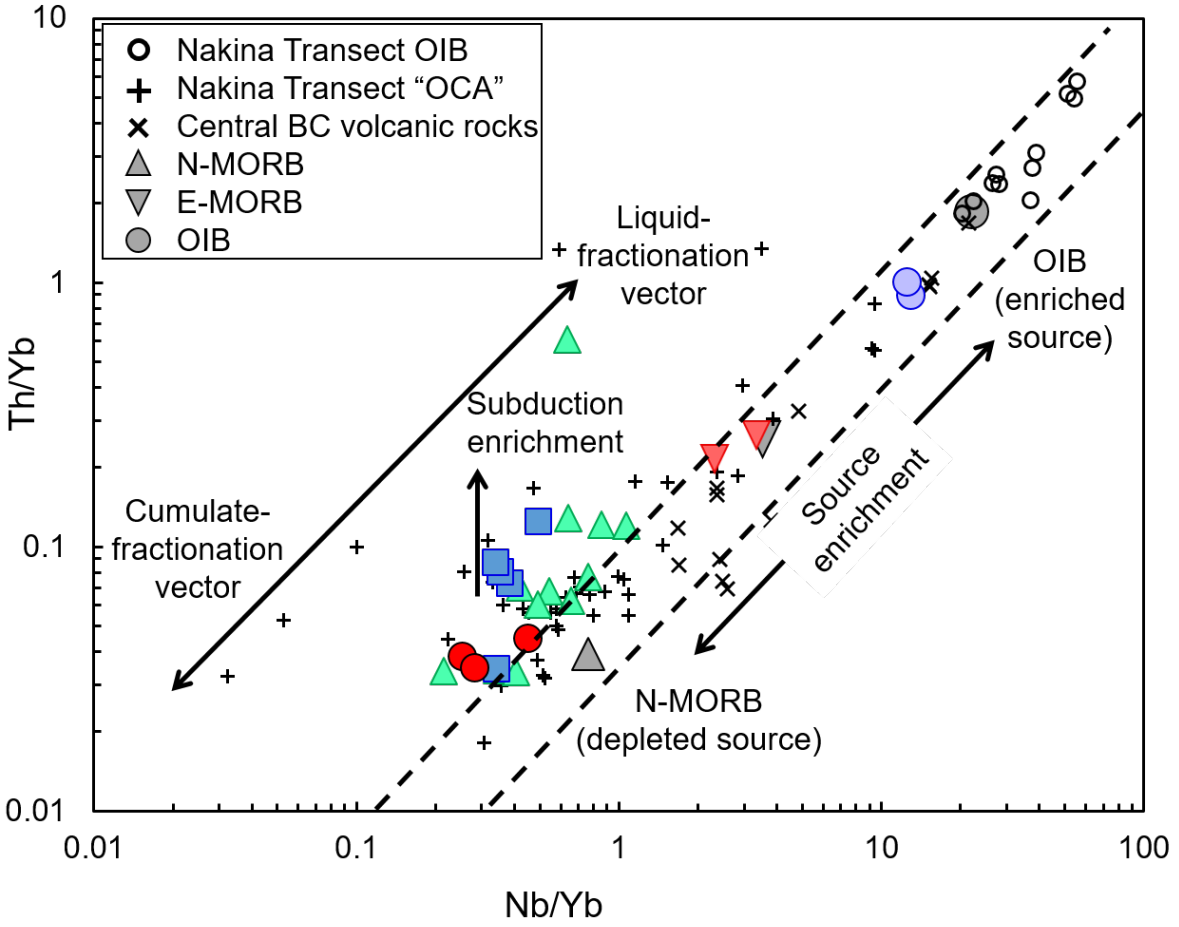
Nakina Transect OIB
Nakina Transect "OCA"
Central BC volcanic rocks
N-MORB
E-MORB
OIB
Liquid-fractionation vector
Subduction enrichment
Cumulate-fractionation vector
Source enrichment
OIB (enriched source)
N-MORB (depleted source)
Th/Yb
Nb/Yb
10
1
0.1
0.01
0.01
0.1
1
10
100

Figure 10

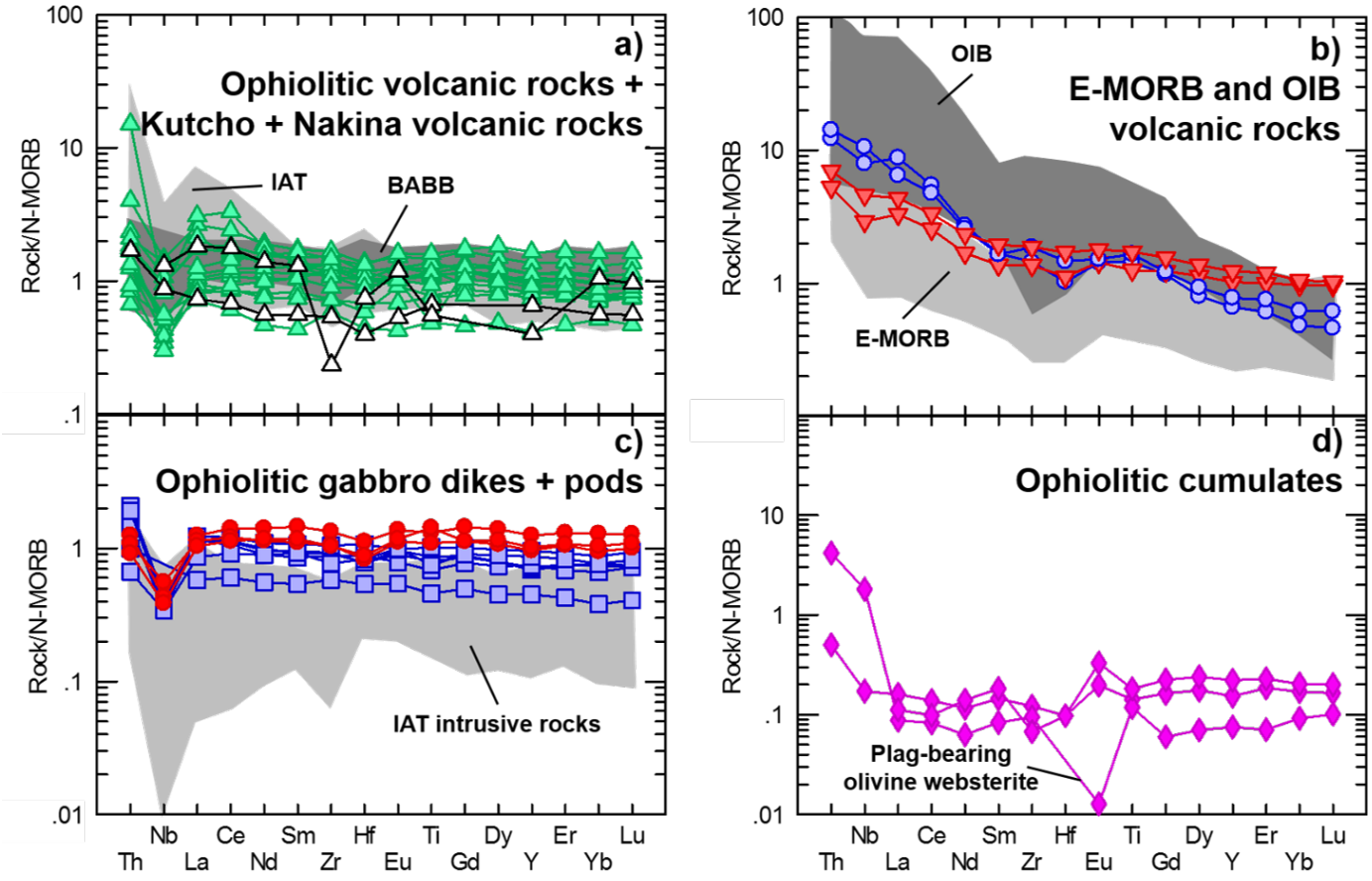
a)
Ophiolitic volcanic rocks +
Kutcho + Nakina volcanic rocks
IAT
BABB
b)
E-MORB and OIB
volcanic rocks
OIB
E-MORB
c)
Ophiolitic gabbro dikes + pods
IAT intrusive rocks
d)
Ophiolitic cumulates
Plag-bearing
olivine websterite
Rock/N-MORB
100
10
1
.1
.01
Th La Nd Zr Eu Gd Y Yb
Nb Ce Sm Hf Ti Dy Er Lu

Figure 11

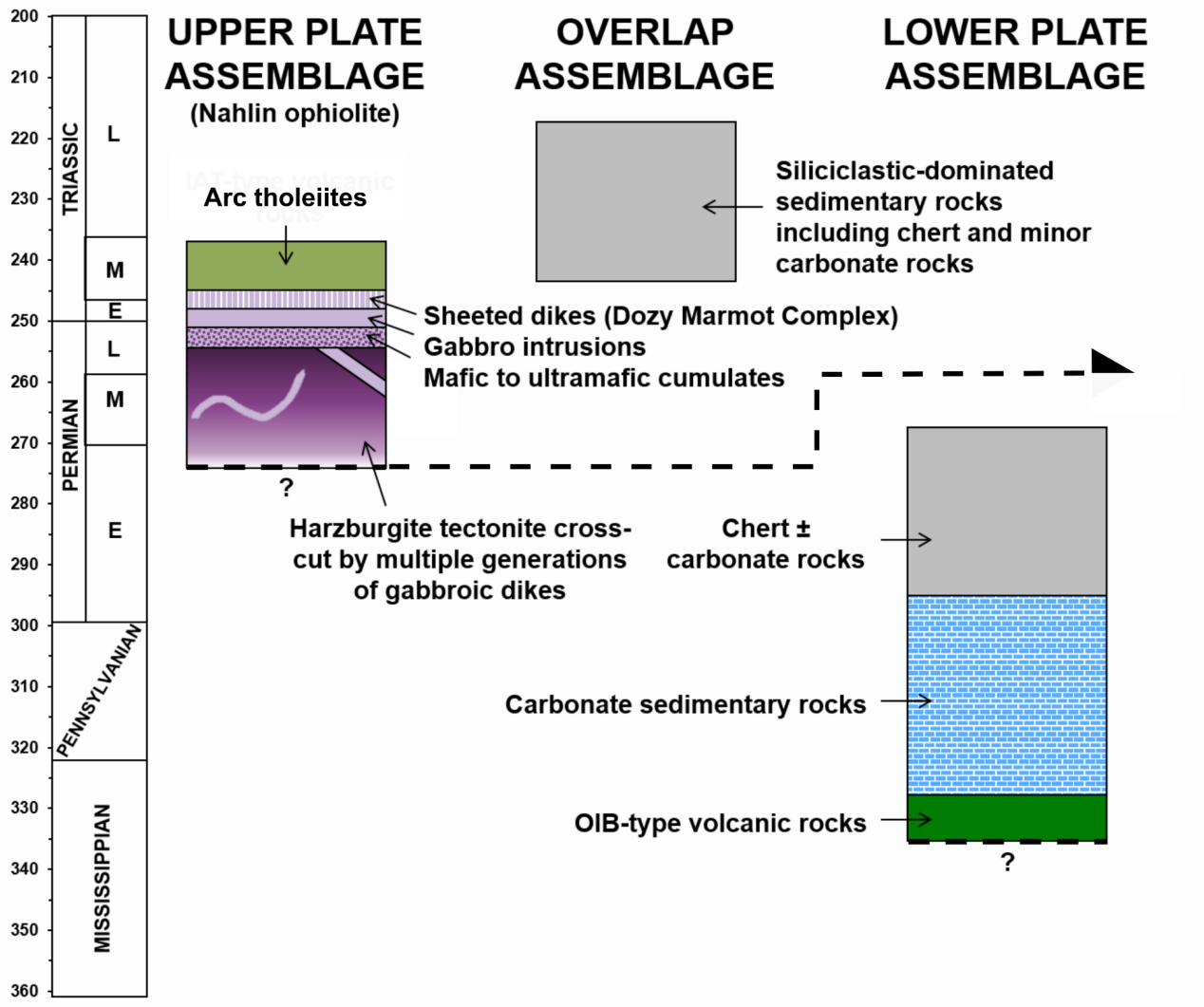
200
210
220
230
240
250
260
270
280
290
300
310
320
330
340
350
360
TRIASSIC
L
M
E
PERMIAN
L
M
E
PENNSYLVANIAN
MISSISSIPPIAN
UPPER PLATE ASSEMBLAGE
(Nahlin ophiolite)
OVERLAP ASSEMBLAGE
LOWER PLATE ASSEMBLAGE
Arc tholeiites
Siliciclastic-dominated sedimentary rocks including chert and minor carbonate rocks
Sheeted dikes (Dozy Marmot Complex)
Gabbro intrusions
Mafic to ultramafic cumulates
?
Harzburgite tectonite cross-cut by multiple generations of gabbroic dikes
Chert ± carbonate rocks
Carbonate sedimentary rocks
OIB-type volcanic rocks
?

Figure 12

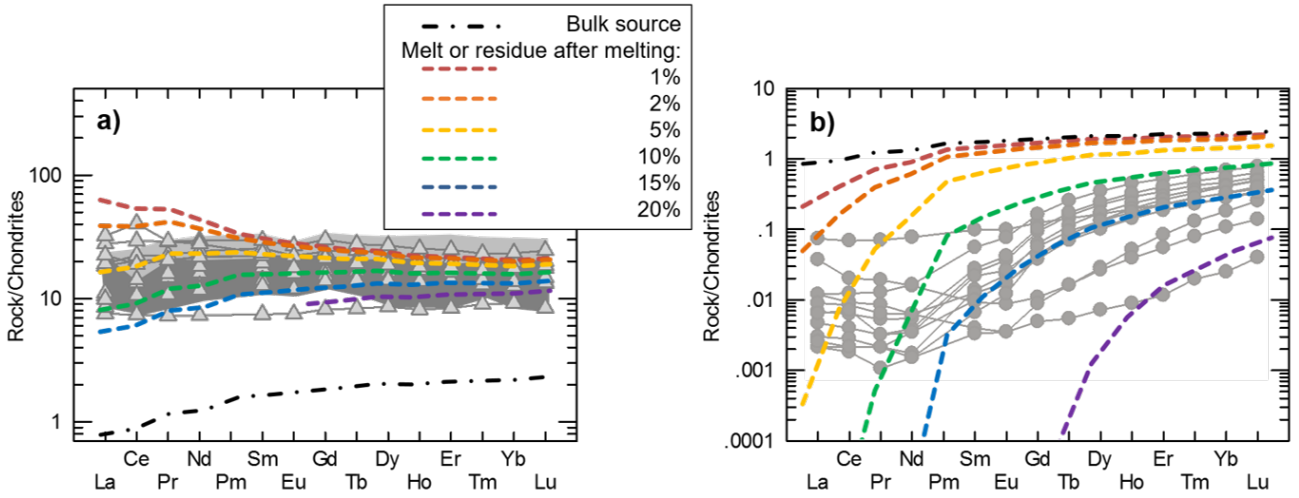
Bulk source
Melt or residue after melting:
1%
2%
5%
10%
15%
20%
a)
b)
Rock/Chondrites
100
10
1
.1
.01
.001
.0001
La Ce Pr Nd Pm Sm Eu Gd Tb Dy Ho Er Tm Yb Lu

Figure 13

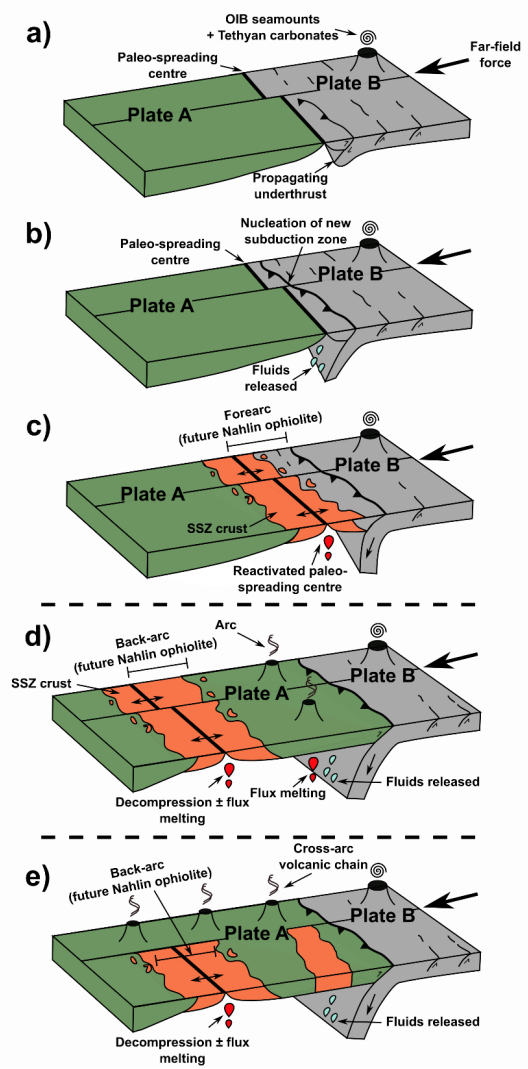
a)
OIB seamounts
+ Tethyan carbonates
Far-field
force
Paleo-spreading
centre
Plate B
Plate A
Propagating
underthrust
b)
Nucleation of new
subduction zone
Paleo-spreading
centre
Plate B
Plate A
Fluids
released
c)
Forearc
(future Nahlin ophiolite)
Plate B
Plate A
SSZ crust
Reactivated paleo-
spreading centre
d)
Back-arc
(future Nahlin ophiolite)
Arc
SSZ crust
Plate B
Plate A
Fluids released
Flux melting
Decompression ± flux
melting
e)
Back-arc
(future Nahlin ophiolite)
Cross-arc
volcanic chain
Plate B
Plate A
Fluids released
Decompression ± flux
melting

Table 2 - Supplemental - Lithogeochemical Data for Igneous Rocks of the Menetatauline Area

Sample	15ZE-0943	15ZE-0944	15ZE953	15ZE955	15ZE-0985	ZE15SM030
Latitude	58.921	58.915	58.878	58.881	60.328	58.935
Longitude	-132.294	-132.291	-132.371	-132.381	-133.323	-132.260
Rock type	Mafic volcanic	Mafic volcanic	Mafic volcanic	Mafic volcanic	Mafic volcanic	Mafic volcaniclastic
Affinity	IAT	IAT	IAT	IAT	IAT	IAT
SiO2	50.17	51.13	52.81	59.62	52.01	51.08
Al2O3	15.43	14.93	15.60	15.85	14.30	14.70
Fe2O3	10.80	10.28	13.11	10.33	13.79	10.68
MnO	0.17	0.17	0.10	0.14	0.22	0.16
MgO	6.47	8.37	8.39	4.78	5.21	8.70
CaO	12.63	10.30	4.14	2.53	7.63	9.09
Na2O	2.62	3.00	2.50	5.99	4.07	3.79
K2O	0.12	0.55	1.77	0.07	0.54	0.27
TiO2	1.45	1.18	1.49	0.62	2.02	1.36
P2O5	0.13	0.11	0.10	0.06	0.19	0.14
Cr2O3	0.04	0.05	0.03	0.01	0.02	0.05
Total	100.00	100.01	100.00	99.99	99.99	99.98
Cs	n.d.	0.3	1.1	0.2	4.5	0.3
Rb	2	12	22	n.d.	14	5
Sr	49	38	194	25	97	81
Ba	14	34	301	17	781	20
Y	31.4	25.3	22.5	11.5	45.9	27.2
Zr	79	66	92	43	108	97
Hf	2.1	1.8	2	0.9	2.7	2.1
Nb	0.7	1.3	1.2	1	3.2	2.2
Ta	0.14	0.37	0.04	0.04	0.37	0.13
Sc	41	35	35	32	41	37
V	318	264	366	184	393	288
Ni	80	190	130	40	70	180
Cu	70	60	50	n.d.	80	80
Zn	80	70	90	70	120	90
W	n.d.	1.8	0.6	0.6	1.8	0.7
As	n.d.	n.d.	n.d.	n.d.	n.d.	n.d.
Tl	n.d.	0.08	n.d.	n.d.	0.14	n.d.
Pb	n.d.	n.d.	n.d.	n.d.	n.d.	n.d.
Th	0.11	0.16	0.15	0.2	0.25	0.22
U	0.18	0.11	0.09	0.15	0.14	0.14
La	2.81	2.03	2.49	1.78	3.14	4.35
Ce	9.2	6.91	8.17	4.53	10.8	12.4
Pr	1.57	1.29	1.4	0.69	1.99	1.94
Nd	9.13	7.22	7.5	3.4	11.2	10.1
Sm	3.36	2.76	2.72	1.14	4.36	3.38
Eu	1.29	1.04	1.05	0.433	1.64	1.06
Gd	4.68	3.8	3.49	1.68	6.37	4.34
Tb	0.88	0.71	0.62	0.31	1.15	0.76
Dy	5.64	4.46	4.13	2.18	8.25	5.11
Ho	1.16	0.95	0.83	0.46	1.69	1.04
Er	3.35	2.69	2.5	1.38	4.93	3.02
Tm	0.501	0.413	0.348	0.229	0.758	0.462
Yb	3.26	2.64	2.22	1.56	4.95	2.87
Lu	0.52	0.404	0.336	0.213	0.739	0.447

ZE15SM031A	ZE15SM039B	ZE15SM040	ZE15SM105	16SM 167	16SM 172	ZE15SM033
58.932	58.962	58.959	58.964	58.885	58.869	58.936
-132.257	-132.214	-132.212	-132.734	-132.188	-132.167	-132.246
Mafic volcaniclastic	Mafic volcanic	Mafic volcaniclastic	Mafic volcanic	Ultramafic volcaniclastic	Mafic volcaniclastic	Diabasic dike
IAT	IAT	IAT	IAT	IAT	IAT	IAT
50.50	50.68	51.19	47.57	47.71	50.03	54.62
16.05	14.38	15.01	13.81	8.03	17.14	14.97
8.88	10.63	10.87	13.48	12.16	15.40	11.55
0.15	0.18	0.18	0.22	0.24	0.27	0.16
7.08	8.22	6.72	5.61	20.58	3.74	4.52
14.23	11.93	10.80	13.18	9.91	6.53	8.03
1.85	2.04	3.39	3.87	0.30	4.34	4.78
0.20	0.21	0.33	0.25	0.02	0.68	0.15
0.98	1.56	1.41	1.85	0.96	1.73	1.10
0.06	0.16	0.10	0.19	0.09	0.15	0.10
0.04	0.05	0.02	0.02	0.20	0.09	0.01
99.99	99.99	100.01	100.03	100.00	100.00	100.00
0.1	0.1	0.2	0.2	0.2	0.4	n.d.
3	4	3	2	n.d.	13	2
53	151	94	424	18	90	137
9	9	49	149	9	124	19
20.7	31.6	28	37.9	22.7	26.3	19.3
54	114	81	123	53	88	68
1.2	2.4	1.8	2.8	1.4	2.4	1.6
0.8	2.2	1.2	3.4	0.9	2.5	0.9
n.d.	0.11	0.04	0.19	0.07	0.19	0.02
36	35	37	37	39	33	34
261	303	317	379	229	277	359
110	170	70	60	460	280	40
70	50	60	60	40	70	60
60	60	80	100	110	210	90
0.6	n.d.	0.5	n.d.	n.d.	n.d.	n.d.
n.d.	n.d.	n.d.	n.d.	n.d.	10	n.d.
n.d.	n.d.	n.d.	n.d.	n.d.	n.d.	n.d.
n.d.	n.d.	n.d.	7	n.d.	n.d.	28
0.08	0.21	0.1	0.48	0.15	0.28	0.17
0.12	0.12	0.05	0.2	0.18	0.32	0.11
2.02	4.53	2.63	6.58	2.34	5.32	2.88
6.34	13.7	8.69	17.9	6.48	11.6	8.51
1.09	2.13	1.51	2.75	1.02	1.94	1.37
5.9	11.3	8.51	13.8	5.47	10.2	7.27
2.15	3.91	2.98	4.52	1.94	3.39	2.4
0.928	1.29	1.08	1.55	0.694	1.28	0.979
3.17	4.94	4.2	6.16	2.85	4.5	3.23
0.56	0.92	0.76	1.03	0.53	0.76	0.54
3.71	5.81	5.01	6.82	3.57	4.83	3.62
0.8	1.21	1.06	1.43	0.78	0.96	0.77
2.28	3.47	3.07	4.11	2.35	2.69	2.21
0.362	0.506	0.452	0.589	0.33	0.363	0.346
2.34	3.36	2.97	3.96	2.14	2.34	2.34
0.346	0.507	0.471	0.621	0.339	0.375	0.338

ZE15SM054A	16SM 161	16SM 163	16SM 178	16SM 186	ZE15AC062	ZE15SM050
58.948	58.902	58.899	58.863	58.878	58.961	58.971
-132.254	-132.169	-132.171	-132.114	-132.143	-132.764	-132.239
Diabasic dike	Gabbroic dike	Amph-bearing gabbroic dike	Amph-bearing gabbroic dike	Gabbroic dike	Gabbro	Gabbro
IAT	IAT	IAT	IAT	IAT	IAT	IAT
55.21	52.57	55.08	54.28	50.72	53.95	44.25
15.28	16.57	14.91	14.69	16.84	14.14	9.32
11.87	7.89	8.67	11.86	9.20	12.55	10.69
0.17	0.13	0.13	0.20	0.15	0.20	0.19
4.36	7.71	7.26	4.21	7.77	5.23	7.87
8.98	10.03	8.32	8.50	9.78	6.30	21.34
2.87	4.04	4.13	4.76	3.19	5.55	4.74
0.14	0.41	0.52	0.10	1.33	0.21	0.13
1.01	0.58	0.87	1.29	0.95	1.66	1.39
0.10	0.05	0.10	0.13	0.06	0.15	0.13
0.01	0.01	0.02		0.04	0.02	0.04
100.00	99.98	100.00	100.02	100.00	99.95	100.03
n.d.	n.d.	0.1	n.d.	0.1	0.2	0.3
n.d.	7	7	n.d.	14	3	4
162	223	218	171	365	142	27
27	40	51	27	30	24	n.d.
20.2	12.6	20.8	26.7	24.2	35	27
69	43	65	78	57	99	78
1.6	1.1	1.8	2.2	1.7	2.3	1.7
0.8	n.d.	1	0.9	0.8	1	1.3
n.d.	0.01	0.08	0.08	0.06	n.d.	0.05
35	36	32	32	35	33	38
357	185	234	333	227	297	306
30	90	60	40	120	100	120
40	120	60	60	60	40	50
80	50	50	70	60	100	70
0.7	n.d.	n.d.	n.d.	n.d.	0.7	0.7
n.d.	n.d.	n.d.	n.d.	n.d.	n.d.	n.d.
n.d.	n.d.	n.d.	n.d.	n.d.	n.d.	n.d.
n.d.	n.d.	n.d.	n.d.	n.d.	33	n.d.
0.18	0.12	0.25	0.23	0.08	0.15	0.13
0.11	0.07	0.15	0.16	0.04	0.1	0.05
2.87	1.45	2.89	3.08	2.16	3.12	2.85
8.36	4.51	7.95	9.1	6.86	10.6	9.08
1.35	0.77	1.19	1.5	1.14	1.87	1.48
7.06	4.04	6.57	8.03	6.51	10.3	8.35
2.49	1.42	2.25	2.82	2.43	3.83	2.92
0.92	0.554	0.803	1	1.02	1.4	1.14
3.16	1.83	2.86	3.7	3.32	5.32	4.16
0.57	0.31	0.5	0.68	0.61	0.97	0.77
3.6	2.04	3.35	4.47	4.06	6.34	4.89
0.78	0.43	0.71	0.94	0.87	1.33	1.02
2.24	1.26	2.04	2.75	2.48	3.88	3.14
0.356	0.187	0.311	0.404	0.346	0.583	0.458
2.25	1.16	2.02	2.65	2.33	3.93	2.89
0.335	0.185	0.329	0.427	0.373	0.584	0.457

ZE15SM090	15ZE956A	15ZE959A	15ZE965	15ZE971	ZE15SM112A	15ZE-0945
58.973	58.886	58.892	58.899	58.960	58.980	58.912
-132.679	-132.373	-132.390	-132.391	-132.382	-132.698	-132.290
Amph-bearing gabbro	Gabbronorite cumulate	Gabbronorite cumulate	Plag-bearing olivine websterite cumulate	Mafic volcanic	Mafic volcanic	Mafic volcanic
IAT	IAT	IAT	IAT	OIB	OIB	EMORB
52.12	45.60	49.55	43.47	48.32	40.38	46.56
13.44	15.63	14.22	10.73	16.50	14.09	19.10
13.26	7.36	5.90	3.63	10.33	5.90	12.24
0.20	0.13	0.11	0.03	0.18	0.07	0.21
5.76	11.99	13.22	36.56	7.15	3.66	7.04
8.39	18.57	15.48	5.24	11.83	27.40	11.05
4.47	0.42	1.28	0.18	3.16	3.58	1.58
0.45	0.04	0.06	0.01	0.19	2.12	0.45
1.81	0.23	0.18	0.15	2.10	1.84	1.59
0.09	-	0.01	-	0.25	0.95	0.18
0.02	0.08	0.11	0.56	0.01	0.04	0.05
99.99	99.98	100.02	100.01	100.02	99.98	100.00
0.5	n.d.	n.d.	n.d.	0.6	2.7	0.2
6	n.d.	n.d.	n.d.	7	35	10
118	257	323	4	136	159	620
24	12	13	4	43	275	44
28.5	6.2	4.3	2.1	21.7	18.5	28.5
77	5	9	7	138	107	101
1.8	0.2	0.2	n.d.	3	2.1	2.3
0.9	n.d.	0.4	4.2	24.6	18.5	6.8
n.d.	0.04	n.d.	0.05	2.12	1.27	0.6
37	40	41	11	36	20	46
474	138	150	74	277	160	274
90	240	320	1110	60	80	140
40	130	80	10	100	40	90
90	40	n.d.	n.d.	80	40	130
n.d.	n.d.	n.d.	0.6	1.8	1.1	n.d.
n.d.	n.d.	n.d.	n.d.	9	n.d.	n.d.
n.d.	n.d.	n.d.	n.d.	n.d.	0.07	0.07
n.d.	n.d.	35	11	n.d.	n.d.	n.d.
0.11	n.d.	0.06	0.5	1.7	1.47	0.63
0.07	n.d.	0.02	0.01	0.5	0.52	0.26
2.6	0.28	0.4	0.22	16.2	21.9	8.25
8.51	0.74	1.04	0.62	35.7	40.9	19.1
1.44	0.15	0.15	0.11	4.45	4.67	2.61
8.6	1.02	0.85	0.46	18.7	19.8	12.3
3.09	0.48	0.38	0.22	4.34	4.41	3.61
1.2	0.335	0.201	0.013	1.55	1.46	1.47
4.17	0.82	0.6	0.22	4.47	4.27	4.53
0.81	0.16	0.11	0.04	0.7	0.62	0.79
5.23	1.09	0.8	0.32	4.23	3.64	5.18
1.09	0.25	0.18	0.07	0.79	0.66	1.06
3.2	0.68	0.55	0.21	2.23	1.81	2.98
0.487	0.101	0.083	0.037	0.329	0.235	0.443
3.18	0.62	0.52	0.28	1.9	1.47	2.95
0.498	0.091	0.075	0.046	0.279	0.21	0.438

15ZE-0972								
58.962								
-132.374	Standards							
Mafic volcanic	DNC-1			OREAS 101B			W-2a	
EMORB	Certified	Measured	% accuracy	Certified	Measured	% accuracy	Certified	Measured
48.78	47.15	47.26	0.23				52.40	52.31
15.86	18.34	17.67	3.65				15.40	15.37
13.49	9.97	9.43	5.42				10.70	10.64
0.24	0.15	0.15	2.67				0.16	0.17
5.77	10.13	9.74	3.85				6.37	6.45
9.90	11.49	11.44	0.44				10.90	10.95
3.02	1.89	1.93	2.12				2.14	2.17
0.49	0.23	0.22	5.98				0.63	0.60
2.19	0.48	0.47	1.88				1.06	1.08
0.27	0.07	0.07	0.00				0.13	0.13
0.03	0.04	0.04	3.70				0.01	0.01
100.01	99.90	98.38					99.89	99.86
0.6								
11							21	20
114	144	139	3.5				190	192
116	118	102	13.6				182	170
34.4	18	17.7	1.7	178	180	1.1	24	21.7
139	38	37	2.6				94	95
3.5							2.6	2.5
10.7							7.9	7.3
0.92								
43	31	31	0.0				36	35
330	148	157	6.1				262	267
130	247	270	9.3	9	< 20		70	70
60	100	100	0.0	416	420	1.0	110	110
170							80	90
1.9							0.3	< 0.5
n.d.								
0.1							0.2	0.06
n.d.								
0.84				37.1	39.8	6.8	2.4	2.5
0.22				396	426	7.0	0.53	0.55
10.9				789	820	3.9		
25				1331	1430	7.4	23	24.8
3.64				127	129	1.6		
17.1				378	389	2.9	13	13.3
5.12				48	50	4.2	3.3	3.4
1.83	0.59	0.63	6.8	7.77	8.34	7.3		
5.73								
1				5.37	5.46	1.7	0.63	0.64
6.24				32.1	32.5	1.2		
1.27				6.34	6.44	1.6	0.76	0.81
3.57				18.7	19.4	3.7	2.5	2.3
0.505				2.66	2.82	6.0		
3.21	2	2.1	5.0	17.6	18.2	3.4	2.1	2.1
0.468				2.58	2.63	1.9	0.33	0.32

% accuracy
0.17
0.19
0.56
1.23
1.26
0.46
1.40
4.15
1.51
0.00
8.70
4.8
1.1
6.6
9.6
1.1
3.8
7.6
2.8
1.9
0.0
0.0
12.5
70.0
4.2
3.8
7.8
2.3
3.0
1.6
6.6
8.0
0.0
3.0

Standard	DNC-1			OREAS 101B			W-2a		
	Certified	Measured	% accuracy	Certified	Measured	% accuracy	Certified	Measured	% accuracy
SiO2	47.15	47.26	0.23				52.40	52.31	0.17
Al2O3	18.34	17.67	3.65				15.40	15.37	0.19
Fe2O3	9.97	9.43	5.42				10.70	10.64	0.56
MnO	0.15	0.15	2.67				0.16	0.17	1.23
MgO	10.13	9.74	3.85				6.37	6.45	1.26
CaO	11.49	11.44	0.44				10.90	10.95	0.46
Na2O	1.89	1.93	2.12				2.14	2.17	1.40
K2O	0.23	0.22	5.98				0.63	0.60	4.15
TiO2	0.48	0.47	1.88				1.06	1.08	1.51
P2O5	0.07	0.07	0.00				0.13	0.13	0.00
Cr2O3	0.04	0.04	3.70				0.01	0.01	8.70
Total	99.90	98.38					99.89	99.86	
Cs									
Rb							21	20	4.8
Sr	144	139	3.5				190	192	1.1
Ba	118	102	13.6				182	170	6.6
Y	18	17.7	1.7	178	180	1.1	24	21.7	9.6
Zr	38	37	2.6				94	95	1.1
Hf							2.6	2.5	3.8
Nb							7.9	7.3	7.6
Ta									
Sc	31	31	0.0				36	35	2.8
V	148	157	6.1				262	267	1.9
Cr	270	280	3.7				92	100	8.7
Ni	247	270	9.3	9	< 20		70	70	0.0
Cu	100	100	0.0	416	420	1.0	110	110	0.0
Zn							80	90	12.5
W							0.3	< 0.5	
As									
Tl							0.2	0.06	70.0
Pb									
Th				37.1	39.8	6.8	2.4	2.5	4.2
U				396	426	7.0	0.53	0.55	3.8
La				789	820	3.9			
Ce				1331	1430	7.4	23	24.8	7.8
Pr				127	129	1.6			
Nd				378	389	2.9	13	13.3	2.3
Sm				48	50	4.2	3.3	3.4	3.0
Eu	0.59	0.63	6.8	7.77	8.34	7.3			
Gd									
Tb				5.37	5.46	1.7	0.63	0.64	1.6

Dy				32.1	32.5	1.2			
Ho				6.34	6.44	1.6	0.76	0.81	6.6
Er				18.7	19.4	3.7	2.5	2.3	8.0
Tm				2.66	2.82	6.0			
Yb	2	2.1	5.0	17.6	18.2	3.4	2.1	2.1	0.0
Lu				2.58	2.63	1.9	0.33	0.32	3.0